AD-A153 951 THE APPLICATION OF LASER RESONANCE SATURATION TO THE DEVELOPMENT OF EFFIC..(U) TORONTO UNIV DOWNSVIEW (ONTARIO) INST FOR AEROSPACE STUDIES R M MEASURES

UNCLASSIFIED 31 OCT 84 AFOSR-TR-85-0376 AFOSR-80-0057 F/G 20/5 NL

1/1

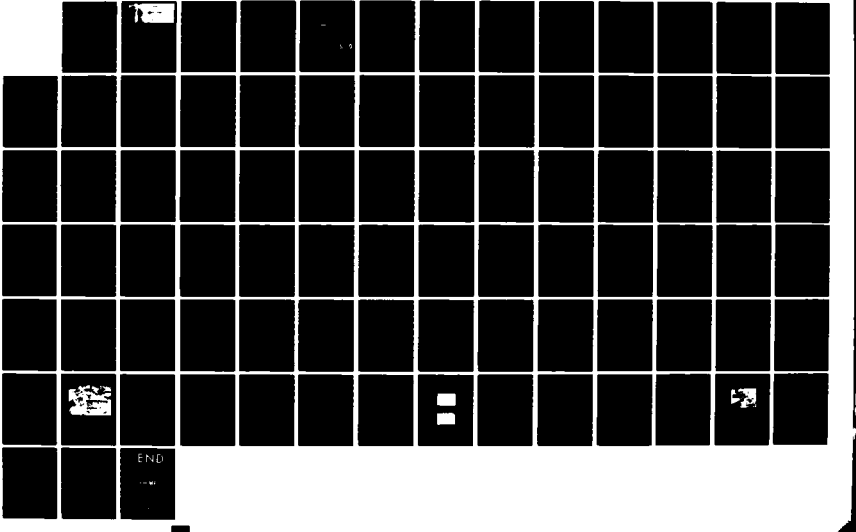

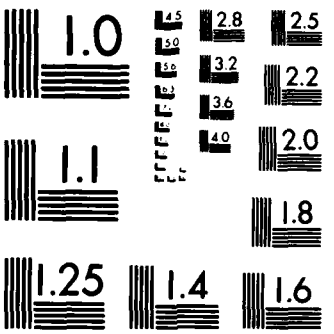

MICROCOPY RESOLUTION TEST CHART
NATIONAL BUREAU OF STANDARDS-1963-A

INSTITUTE FOR AEROSPACE STUDIES

UNIVERSITY OF TORONTO

THE APPLICATION OF LASER RESONANCE SATURATION TO THE DEVELOPMENT OF EFFICIENT SHORT WAVELENGTH LASERS

Final Technical Report

(for period ending October 31, 1984)

US AFOSR 80-0057D

Prepared by

Dr. R. M. Measures
Institute for Aerospace Studies
University of Toronto
4925 Dufferin Street
Downsview, Ontario, Canada
M3H 5T6

SECURITY CLASSIFICATION OF THIS PAGE (When Data Entered)

REPORT DOCUMENTATION PAGE		READ INSTRUCTIONS BEFORE COMPLETING FORM
1. REPORT NUMBER AFOSR-TR- 85-0376	2. GOVT ACCESSION NO. AD-A153951	3. RECIPIENT'S CATALOG NUMBER
4. TITLE (and Subtitle) THE APPLICATION OF LASER RESONANCE SATURATION TO THE DEVELOPMENT OF EFFICIENT SHORT WAVELENGTH LASERS		5. TYPE OF REPORT & PERIOD COVERED Final Report 1 Oct 79 - 31 Oct 84 6. PERFORMING ORG. REPORT NUMBER
7. AUTHOR(s) Dr. R. M. Measures		8. CONTRACT OR GRANT NUMBER(s) AFOSR 80-0057
9. PERFORMING ORGANIZATION NAME AND ADDRESS University of Toronto, Institute for Aerospace Studies, 4925 Dufferin Street, Downsview, Ontario, Canada, M3H 5T6		10. PROGRAM ELEMENT, PROJECT, TASK AREA & WORK UNIT NUMBERS 61102F 2301/A8
11. CONTROLLING OFFICE NAME AND ADDRESS Air Force Office of Scientific Research/ Bldg. 410, Bolling Air Force Base, DC 20332, USA		12. REPORT DATE 31 Oct 84 13. NUMBER OF PAGES 81
14. MONITORING AGENCY NAME & ADDRESS(if different from Controlling Office) AFOSR/NP Building 410 Bolling AFB DC 20332-6448		15. SECURITY CLASS. (of this report) Unclassified 15a. DECLASSIFICATION/DOWNGRADING SCHEDULE

16. DISTRIBUTION STATEMENT (of this Report)

Approved for public release; distribution unlimited.

17. DISTRIBUTION STATEMENT (of the abstract entered in Block 20, if different from Report)

18. SUPPLEMENTARY NOTES

19. KEY WORDS (Continue on reverse side if necessary and identify by block number)

1. XUV-ray lasers, 2. Sodium plasma, 3. Laser resonance saturation, 4. Laser ionization, 5. Electron temperature measurement, 6. Stark broadening, 7. Electron density measurements, 8. Three photon saturation, 9. Atom density measurements, 10. Laser diagnostics, 11. Alkali oven, 12. Superelastic plasma heating.

20. ABSTRACT (Continue on reverse side if necessary and identify by block number)

Laser saturation of an atomic resonance transition represents an important new mode of coupling laser energy into a gas or plasma. The basic mechanism in either case is superelastic collisional heating of free electrons. For a gas various seed ionization processes precede this interaction. During the past year we have developed a computational code for mapping the three dimensional nature of this interaction. This is required because this strong interaction invariably distorts and attenuates

DD FORM 1 JAN 73 1473 EDITION OF 1 NOV 65 IS OBSOLETE

UNCLASSIFIED

SECURITY CLASSIFICATION OF THIS PAGE (When Data Entered)

the laser pulse as it propagates through the medium being excited. We have also developed a new experimental facility for studying this interaction and have recently completed our first spectroscopic measurements of the electron temperature produced in a sodium plasma created through laser resonance saturation. This temperature appears to be somewhat lower than predicted by our computer simulation and we are currently attempting to reconcile this difference. Also within the past year we have discovered that attenuation of the laser pulse is a maximum when the laser is detuned by about 0.5 nm from either of the resonance lines. This result is also predicted by our computer code and appears to represent further confirmation of the importance of laser energy extraction through superelastic electron heating. Recently, we have initiated a study of a new approach to the development of a short wavelength laser based on three photon excitation of an ion with a low lying metastable state.

THE APPLICATION OF LASER RESONANCE SATURATION TO THE DEVELOPMENT OF EFFICIENT SHORT WAVELENGTH LASERS

FINAL Technical Report

(for period ending October 31, 1984

US AFOSR 80-0057D

Prepared by

Dr. R. M. Measures
Professor of Applied Science and Engineering

University of Toronto
Institute for Aerospace Studies
4925 Dufferin Street
Downsview, Ontario, Canada
M3H 5T6

Abstract

Laser saturation of an atomic resonance transition represents an important new mode of coupling laser energy into a gas or plasma. The basic mechanism in either case is superelastic collisional heating of free electrons. For a gas various seed ionization processes precede this interaction. During the past year we have developed a computational code for mapping the three dimensional nature of this interaction. This is required because this strong interaction invariably distorts and attenuates the laser pulse as it propagates through the medium being excited. We have also developed a new experimental facility for studying this interaction and have recently completed our first spectroscopic measurements of the electron temperature produced in a sodium plasma created through laser resonance saturation. This temperature appears to be somewhat lower than predicted by our computer simulation and we are currently attempting to reconcile this difference. Also within the past year we have discovered that attenuation of the laser pulse is a maximum when the laser is detuned by about 0.5 nm from either of the resonance lines. This result is also predicted by our computer code and appears to represent further confirmation of the importance of laser energy extraction through superelastic electron heating. Recently, we have initiated a study of a new approach to the development of a short wavelength laser based on three photon excitation of an ion with a low lying metastable state.

Contents

RESEARCH OBJECTIVES

Laser saturation of an atomic resonance transition represents an important form of laser-plasma interaction. Even in the case of a neutral atomic vapor laser resonance saturation gives rise to many processes that quickly lead to ionization. Once an appreciable degree of ionization has been achieved the primary mechanism for converting laser energy into plasma energy is superelastic electron collision quenching of the laser pumped resonance state population. This is an extremely efficient process which, in effect, rapidly cycles the bound electron between the ground and resonance state, transforming one laser photon into an equivalent amount of free electron kinetic energy during each cycle, see Fig. 1.

Laser resonance saturation can be viewed as complementary to inverse bremsstrahlung, for although it can lead to energy deposition that is many orders of magnitude greater than attainable through inverse bremsstrahlung for modest values of laser irradiance — the free electron temperature achieved is limited by the characteristics of the atom or ion being irradiated. However, laser resonance saturation can lead to extremely rapid electron heating, in effect, creating a well defined electron temperature jump and a commensurate sharp burst in the emission of short wavelength radiation from a suitable plasma.

The objective of our research progam is to study this new form of laser-plasma interaction and explore some of its potential applications. In any practical application the laser has to propagate through a finite depth of the medium being irradiated and as a result of the strong nature of the resonance interaction the laser pulse will undergo an appreciable degree of attenuation and temporal and spatial distortion. Consequently, any theoretical modeling of this interaction should take account of this fact.

To date we are the first to develop a computational analysis that attempts to model the three dimensional nature of this interaction by taking account of the attenuation and distortion suffered by the laser pulse as it burns its way through a realistic atomic vapor distribution. In order to assess the reliability of our theoretical work we are comparing our computer simulations with the results attained from experiments involving a new facililty.

Multiphoton saturation of atomic transitions within a plasma represents the logical extension of this work and we have initiated a new program to consider one possible application of this interaction. This work involves examining the feasibility of a new approach to the development of a short wavelength laser based on three photon saturation of an ion containing a low lying metastable level.

STATUS REPORT

Lasers have been used to create and heat plasma almost since their inception. In the past inverse bremsstrahlung has represented the primary means of heating the free electrons of a plasma. Unfortunately, the small cross section involved in this interaction has limited laser heating to high density plasmas. By contrast laser resonance saturation involves a very large cross section so that efficient coupling of laser energy can be achieved at much lower densities. In this section we shall report on our work to study laser resonance saturation and explore its uses.

Laser Ionization Based on Resonance Saturation (LIBORS)

An intense laser field of appropriate wavelength can lock the populations of the ground and resonance states in the ratio of their degeneracies in an extremely short time. This laser saturation when applied to an atomic resonance transition has been shown [1-7] to produce near full ionization and there is now substantial support for our idea that the primary mechanism for coupling the laser radiation to the free electrons is superelasic collision quenching of the laser pumped resonance state.[8-14] As first pointed out by the author[15,16] the resonance transition, in effect, behaves as an extremely efficient engine that converts laser energy into kinetic energy of the free electrons, see Fig. 1.

We have shown theoretically[17-20] that this new form of laser-plasma interaction should lead to a jump in the free electron temperature that is independent of laser irradiance (provided it is adequate to maintain resonance saturation) and limited in magnitude by the characteristics of the atom or ion being excited. The risetime for the temperature is principally determined by the density of the plasma. An attractive feature of superelastic heating is the efficient production of a concomitant flash

of intense line radiation. This high efficiency is inherent in the mechanism that limits the rise in the free electron temperature — that is to say a dynamic balance between electron superelastic and inelastic collisions. The former heat the free electrons while the latter excite higher energy levels at the expense of energy from the free electrons. In effect, the laser energy is being converted into intense line radiation with high efficiency.

The wavelength of this radiation can be very much shorter than the wavelength of the saturating laser if the selected ion has an appropriate energy level structure. Members of the Li-isoelectronic series (BeII, BIII, CIV, NV, OVI, ...) are near ideal as they possess a large energy gap between their first and second resonance levels.* Table 1 displays the wavelengths of the two lowest resonance transitions for several members of this series indicating clearly that the wavelength of the intense line emission would be very much shorter than that of the saturating laser. This photon energy gain factor ($\lambda_{21}/\lambda_{31}$) can be seen to increase progressively with the members of the series. We have also shown[21] that the magnitude of the temperature jump achieved through resonance saturation increases in a similar manner.

Table 1

Resonance Lines of the Li-Isoelectronic Series

and Photon Energy Gain Factor ($\lambda_{21}/\lambda_{31}$)

	BeII	BIII	CIV	NV	OVI
λ_{31}	103.6 nm	51.8 nm	31.2 nm	20.9 nm	15.0 nm
λ_{21}	313 nm	207 nm	155 nm	124 nm	103 nm
$\lambda_{21}/\lambda_{31}$	3.0	4.0	4.97	5.93	6.87

It is worth noting at this point that the selection of wavelengths attainable through superelastic heating is not restricted to those

* We are neglecting the fine structure of the levels in this statement.

associated with the members of this series for they could be used as a source of temperature jump within a plasma and another species serve to provide the specific line radiation required.

We believe that this new kind of efficient and controlled "intense short wavelength line emission" (ISLE)-source could be used in many ways towards the development of short wavelength (EUV to X-ray) lasers. For example, in the approach of Caro et al[22] an ISLE-source that is tailored to provide primarily radiation at 18.7 nm (as opposed to the broadband source they used) would avoid excitation of the Li states that subsequently autoionize to the Li^+ ground state and destroy the chance of creating a population inversion. A suitably chosen ISLE-source would also be ideal for the selective autoionization proposal of Bokor et al.[23]

Three Dimensional Modeling of LIBORS

In order to better understand laser ionization based on resonance saturation we have undertaken the first theoretical treatment that attempts to model the three dimensional nature of the interaction and includes such real effects as: laser pulse attenuation, non-uniform density distribution along the path of the laser pulse and spectral detuning of the laser.

In our original formulation of the LIBORS computer code we assumed a step-like laser pulse.[17-30] This approximation is reasonable for the incident laser pulse because the time to saturate the resonance transition is very short,[15,20] typically much less than 1 nsec. However, in an actual experiment the laser pulse propagates through a non-uniform atom density distribution and suffers appreciable attenuation. This can lead to a considerable temporal and spatial distortion of the laser pulse. Consequently, the atoms at different locations along the path of the laser pulse are subject to progressively less energy and to a shorter period of excitation.

5-Level LIBORS Computer Code

In an attempt to keep the analysis economically viable we have replaced our 20-level model[17-20] of the sodium atom with the simplified 5-level model shown in figure 2. Although 5-levels are indicated in figure 2, we assume that the collisional coupling between levels 3, 4 and 5 is sufficiently rapid that their populations are more or less in a Boltzmann

equilibrium. This assumption permits us to treat this trio of levels as a manifold and thereby reduce the number of atomic level rate equations to three. In effect we consider only the collisional-radiative processes "into" and "out of" this (3-4-5) manifold.

The remaining 15 high lying energy levels (not shown in figure 2) are partially taken into account by assuming that electron excitation to them from any of the five lower levels leads, in effect, to immediate ionization of the atom. We therefore introduce the 5-level "effective" electron collisional ionization rate coefficient for each of the low lying levels (m = 1 to 5) defined by the relation

$$K^*_{mc} = \sum_{n=6}^{21} K_{mn} \qquad (1)$$

where K_{mn} represents the electron collisional rate coefficient between levels m and n, as used in our LIBORS computer code.[17-20] Note that K_{m21} is the m-level electron ionization rate coefficient according to the 20-level model of the sodium atom. The corresponding "effective" three body recombination rate coefficient to each of the low lying levels (m = 1 to 5) is similarly constituted to take account of recombination to the higher levels, followed by a rapid cascade down to the lower levels, we thus write

$$K^*_{cm} = \sum_{n=6}^{20} K_{cn} p(n,m) \qquad (2)$$

where K_{cn} represents the three-body recombination rate coefficient to level n used in our 20-level LIBORS code and p(n,m) is introduced as the effective probability that a captured free electron arriving in level n subsequently decays to level m.

We have found that close agreement can be obtained between the 5 and 20-level LIBORS codes if these probability factors are generally* given by the expression

---

* In order to obtain the close agreement (indicated later) between the 5 and 20-level LIBORS codes it was found necessary to set p(s, 4) = 1, where s = 17, 12 and 8.

$$p(n,m) = \frac{N_e K_{nm} + A_{nm}}{N_e(K_{nm} + K_{nq} + K_{nc}) + A_{nm} + A_{nq}} \qquad (3)$$

where N_e is the free electron density, A_{nm} the Einstein spontaneous transition probability between levels n and m, and q is the level within the manifold that is optically connected to level n.

The 5-level model can thus be described by the following set of equations: first we have the three atomic level population rate equations,

$$\frac{dN_1}{dt} = (N_2 - gN_1)R_{21} + N_2C_{21} + N_5C_{51} + N_e(N_3K_{31} + N_4K_{41}) + N_e{}^2\beta_{c1}$$

$$+ N_e{}^3K^*_{c1} - N_1\left[N_e\left\{\sum_{m=2}^{5} K_{1m} + K^*_{1c}\right\}\right] \qquad (4)$$

$$\frac{dN_2}{dt} = (gN_1 - N_2)R_{21} + N_e(N_1K_{12} + N_5K_{52}) + N_3C_{32} + N_4C_{42} + N_e{}^2\beta_{c2}$$

$$+ N_e{}^3K^*_{c2} - N_2\left[N_e\left\{\sum_{m=3}^{5} K_{2m} + K^*_{2c}\right\} + C_{21}\right] - \frac{1}{2}N_2{}^2v(\sigma_L F + \sigma_A) - N_2\sigma^{(2)}_{2c}F^2 \qquad (5)$$

and

$$\frac{dN^*_3}{dt} = N_e\left[\sum_{m=3}^{5} (N_1K_{1m} + N_2K_{2m} + N_e{}^2K^*_{cm} + N_e\beta_{cm})\right] - N_3(C_{32} + N_eK_{31} + P_{3c})$$

$$- N_4(C_{42} + N_eK_{41} + P_{4c}) - N_5(C_{51} + N_eK_{52} + P_{5c}) \qquad (6)$$

where we have introduced the (3-4-5) level manifold population density

$$N^*_3 = N_3 + N_4 + N_5 \qquad (7)$$

As indicated we assume that the close spacing of these three levels ensures collisional equilibrium and consequently that the internal distribution of this manifold is described by a Boltzmann distribution. In which case

$$N_k = N_3^* / U_k(T_e) \tag{8}$$

where

$$U_k(T_e) = \sum_{m=3,4,5} g_{mk} e^{-E_{mk}/kT_e} \tag{9}$$

with $g_{mk} \equiv g_m/g_k$ and k = 3, 4 or 5. In order to streamline the equations as far as possible we also introduced the notation,

$$C_{nm} = N_e K_{nm} + A_{nm} \tag{10}$$

and

$$P_{nc} = \sigma_{nc} F + N_e K_{nc}^* \tag{11}$$

where σ_{nc} is the single photon ionization cross section for level n and F is the laser photon flux density, i.e.,

$$F(t) = \frac{1}{h\nu} \int I^{\ell}(\nu,t) d\nu \tag{12}$$

where $I^{\ell}(\nu,t)$ is the laser spectral irradiance at time t and $h\nu$ the laser photon energy. In the above equations we have also introduced the resonance to ground level degeneracy ratio g and the stimulated emission rate per resonance state atom,

$$R_{21}(t) = \frac{B_{21}}{4\pi} \int I^{\ell}(\nu,t) L_{21}(\nu) d\nu \tag{13}$$

where B_{21} is the Milne stimulated emission coefficient and $L_{21}(\nu)$ is the line profile function for the resonance transition.

The appropriate electron energy equation can be expressed in the following form:

$$\frac{d}{dt}(N_e\varepsilon_e) = N_e \sum_{\substack{n=2 \\ (n\neq m)}}^{5}\sum_{m=1}^{2} N_n K_{nm} E_{nm} + N_e{}^3 \sum_{m=1}^{5} K^*_{cm} E^{\#}_{cm} + \sum_{m=3}^{5} (E_{21} - E_{cm}) N_m \sigma_{mc} F$$

$$- N_e{}^2 \sum_{n=1}^{5} \beta_{cn}\varepsilon_e - N_e \sum_{\substack{m=1 \\ (n\neq m)}}^{2}\sum_{n=2}^{5} N_m K_{mn} E_{nm} - N_e \sum_{m=1}^{5} N_m K^*_{mc} E_{cm} - N_e{}^2 H_{ei} + S \qquad (14)$$

where ε_e represents the free electron mean thermal energy (taken as $\frac{3}{2} kT_e$), β_{cn} is the radiative recombination rate coefficient appropriate for level n, H_{ei} represents the rate of elastic energy transfer to ions through Coulomb scattering collisions[24] and S corresponds to the source of electron energy arising from the various seed ionization processes, i.e.,

$$S = (2E_{21} - E_{c2})\{N_2 \sigma^{(2)}_{2c} F^2 + \tfrac{1}{2} N_2{}^2 v q_L F\} + \tfrac{1}{2} N_2{}^2 v \sigma_A E_A \qquad (15)$$

Here $\sigma^{(2)}_{2c}$ represents the two photon resonance state ionization coefficient, σ_L the laser induced Penning ionization coefficient, σ_A the associative ionization cross section and E_A the corresponding energy of creation for the electrons liberated by this latter process. v represents the mean atom velocity.

The energy equation is subsequently divided into an ionization equation and an electron temperature equation as discussed in our earlier work.[17-20] It should be noted that another fine adjustment in the form of a small reduction (of about 0.055 eV) in the three-body recombination energy was found to bring the results of the 5-level LIBORS code into excellent agreement with the 20-level code over a wide range of densities. This modified energy is designated $E^{\#}$ in equation (14).

As we shall see shortly the resonance state population density N_2 is critical in establishing the extent of laser attenuation and its value is in turn determined by the free electron temperature T_e. Once appreciable ionization has been attained T_e tends to rise above the low value produced as a result of burnout. This is particularly true at the higher densities ($N_o \gtrsim 10^{16}$ cm^{-2}). The electron-ion exchange term H_{ei} is the primary limit to the growth in T_e. Since H_{ei} is proportional to $(T_e - T_i)$ it is necessary

to also introduce the appropriate ion energy equation

$$\frac{d\varepsilon_i}{dt} = N_e H_{ei} - N_A H_{iA} \qquad (16)$$

where ε_i is the mean thermal energy of the ions (set equal to $\frac{3}{2} kT_i$). The second term in equation (16) takes account of elastic cooling collisions between the sodium ions and the background of argon buffer gas atoms. N_A is the background argon atom density and H_{iA} is the rate of elastic energy exchange between the ions and the background argon atoms, i.e.,

$$H_{iA} = \langle \sigma v \rangle_{iA} \frac{4m_i}{m_A} \left(1 + \frac{m_i T_A}{m_A T_i}\right)^{1/2} k(T_i - T_A) \qquad (17)$$

where $\langle \sigma v \rangle_{iA}$ is the ion-argon collision frequency and T_A the argon atom's translational temperature.

This background density of argon atoms varies across the sodium vapor region such that the sum of the partial pressures equals the pressure of the argon in the water cooled periphery region. The initial vapor temperature at each location is deduced from the optically measured sodium density profile using the vapor pressure curves provided by Nesmeyanov.[25] By a similar argument to that given above it follows that since H_{iA} is proportional to the difference in temperature between the sodium ions and the argon atoms, the latter has also to be computed. This is done by means of an argon energy equation. It should also be noted that an electron-argon elastic energy loss term was also introduced into both the free electron energy equation and the argon energy equation but its relative importance is marginal.

Combining equations (12) and (13) enables us to write

$$R_{21}(z,t) = \frac{\lambda^2}{8\pi\tau_{21}} F(z,t) \int_{-\infty}^{\infty} L^{\ell}(x_{\ell} - x) L_{21}(x)\, dx \qquad (18)$$

where λ is the wavelength and τ_{21} the radiative lifetime of the resonance transition. We have also introduced the spectral distribution function for the laser radiation

$$L^{\ell}(\nu_{\ell}-\nu) \equiv \frac{I^{\ell}(\nu)}{h\nu F} \tag{19}$$

and the dummy frequency variable _

$$x \equiv \nu - \nu_0 \tag{20}$$

where ν_0 is the resonance line centre frequency. For our experiment we can assume a Lorentzian line profile function of the form

$$L_{21}(\nu - \nu_0) = \frac{1}{\pi} \cdot \frac{\gamma_a}{(\nu-\nu_0)^2 + \gamma_a^2} \tag{21}$$

where γ_a is the appropriate HMHW bandwidth (the Stark width in essence). The laser spectral distribution function can well be approximated by a Gaussian

$$L^{\ell}(\nu_{\ell}-\nu) = \frac{1}{\beta_{\ell}\sqrt{\pi}} e^{-[(\nu_{\ell}-\nu)/\beta_{\ell}]^2} \tag{22}$$

and consequently the convolution of the two profiles in (18) can be expressed in the form of a Voigt function,

$$V(\alpha,u) = \frac{\alpha}{\pi^{3/2}} \int_{-\infty}^{\infty} \frac{e^{-y^2}dy}{\alpha^2 + (u-y)^2} \tag{23}$$

where

$$\alpha \equiv \gamma_a/\beta_{\ell}, \quad y \equiv (x_{\ell}-x)/\beta_{\ell}, \quad u \equiv x_{\ell}/\beta_{\ell} \quad \text{and} \quad V(\alpha, u)du = V(\alpha, \nu)d\nu$$

It is important to notice that this Voigt function depends upon α - the ratio of the atomic bandwidth to the laser bandwidth and to the frequency separation of the atomic and laser centre frequencies normalized by the laser bandwidth, i.e.,

$$u = \frac{\nu_\ell - \nu_0}{\beta_\ell} \qquad (24)$$

In the early phase of our work we were interested in comparing our theoretical predictions with experiments based on the use of a Phase-R flashlamp pumped dye laser, the output of which had a duration of about 1 μsec. A good fit to the temporal laser pulse from this system was obtained using the empirical expression

$$F(o,t) = F_{max}(t/400)^{1/2}\exp\{-\tfrac{1}{4}(t/400)^{1.75}\} \qquad (25)$$

where F_{max} is the peak laser photon flux density and t is in nanoseconds. The exponential bandwidth of this laser pulse β_ℓ was measured to be about 10^{11} Hz (corresponding to a full exponential linewidth of around 0.25 nm).

We recognized from the outset that attenuation of the laser pulse could lead to relatively sudden changes in the laser irradiance. Consequently in our comparison of the 5 and 20-level computer codes we used the truncated laser pulse indicated as F in figure 3(a). With a laser pulse of this shape the comparison was tested fairly severely.

The results for a sodium density (N_o) of 10^{16} cm^{-3} are presented in figure 3(a, b and c). It is evident from a comparison of figures 3(a) and 3(b) that N_2/N_1 falls from the saturated value of 3.0 at about the time of ionization burnout even though F is still increasing. This temporal minimum is attributed to the sudden increase in the superelastic quenching rate. It is apparent from figure 3 that the 5-level LIBORS code mirrors almost exactly the predictions of the 20-level code in regard to the temporal behaviour of the various parameters (i.e., N_e, T_e, T_i, N_2 and N_1). We feel that the small (≈ 20%) difference in the lead time between the two sets of curves is quite acceptable. In order to check that this close agreement was not fortuitous to this particular density we ran a comparison at two additional densities (N_o = 5×10^{15} and 4×10^{16} cm^{-3}). The higher density comparison was also run for a much shorter laser pulse, corresponding to our new laser system, and is presented as figure 4. It is evident that the same close agreement is achieved. Similar close agreement was obtained for the lower density comparison.

The close agreement between the two codes, even when the laser irradiance was suddenly truncated, provided us with sufficient confidence to use the 5-level LIBORS code in evaluating the time history of ionization and the attenuation of the laser pulse as it propagates through the extended region of sodium vapor.

Laser Pulse Attenuation Within an Extended Atomic Vapor Region

If we treat the problem as one dimensional the radiative transfer equation governing the propagation of the laser pulse can be written in the form

$$\frac{1}{c}\frac{\partial F}{\partial t} + \frac{\partial F}{\partial z} = (N_2 - gN_1)R_{21} - N_2\sigma_{2c}^{(2)}F^2 - \frac{1}{2}N_2^2 v q_L F - \sum_{m=3}^{5} N_m \sigma_{mc} F \qquad (26)$$

The first term on the right hand side takes account of the loss of laser photons due to absorption in the resonance transition, the second term allows for two photon ionization of the resonance level, the third term involves laser induced Penning ionization of the resonance level and the last term refers to single photon ionization of the levels within the manifold.

For the time scale of interest in our experiments the velocity of light c can be treated as infinite. Under these circumstances (26) is simplified to the steady state form given by

$$\frac{dF}{dz} = (N_2 - gN_1)R_{21} - N_2\sigma_{2c}^{(2)}F^2 - \frac{1}{2}N_2^2 v q_L F - \sum_{m=3}^{5} N_m \sigma_{mc} F \qquad (27)$$

where R_{21} was given by equation (18).

It is quite clear that addressing the problem of laser resonance saturation for an extended vapor region involves the solution of equations: 4, 5, 6, 14, 16 and 27 in both space and time. We decided to tackle this problem by dividing the vapor column along the path of the laser pulse into a series of slices, see figure 5, each of which was assumed to have a uniform atom density equal to the average experimentally measured sodium atom density for that segment of vapor. The thickness of each slice was

initially set at 1 cm although later computer runs used a much finer slice distribution.

Within each slice our 5-level LIBORS computer code was used to evaluate the temporal variation of the various parameters (such as N_e, T_e, T_i, N_3^*, N_2 and N_1) subject to the laser pulse exiting the previous vapor slice. Although attenuation of the laser pulse within each slice is neglected [i.e., we treat F(z,t) as F(t)], the energy extracted within this vapor slice is computed from equation (27) and this loss is taken into account when considering the appropriate laser pulse to use for the subsequent vapor slice.[26]

Representative time histories of the free electron density, the electron temperature and the laser pulse photon flux density at the three locations indicated on the sodium atom density distribution (measured in an actual experiment and displayed in the lower left-hand corner) are presented in figure 6. The incident laser pulse used in this simulation was chosen to closely match that obtained from our new Nd-YAG laser pumped dye laser. An excellent fit to this short laser pulse was provided by the empirical expression

$$F(o, t) = F_p \times 1.79 \times 10^{-2}\, t^{2.08} \exp(-7.9\times10^{-3} t^2) \qquad (28)$$

where t is in nanoseconds, see figure 7. For the computer simulation presented in figure 6, $F_p \approx 8.33\times10^{25}$ photons cm^{-2} sec^{-1}, corresponding to an energy of 60 mJ in 0.157 cm^2 beam cross section, and the laser was assumed to be detuned by 0.14 nm from the 589.0 nm resonance line.

It is quite apparent that at this energy full ionization is predicted across the entire vapor column and that the general shape of the temperature profile should be quite similar at each location — albeit lengthened or shortened in time dependintg upon the location. The time to achieve full ionization is also seen to vary across the vapor column, being a minimum where the density is a maximum.

Unfortunately, the smaller the spectral detuning of the laser from one of the sodium resonance lines the stronger the radiative rates R_{12} and R_{21} and the smaller the time and space step size required for the computer calculations. Experience has indicated that the smallest economically

acceptable value of laser detuning was 0.14 nm for conditions commensurate with our experiments.

The spatial variation of the degree of ionization along the vapor column, irradiated by the laser pulse, predicted at several instants from the onset time of the incident laser pulse (of energy 27 mJ and detuned by 0.14 nm from the 589.0 nm sodium resonance line) is displayed in figure 8. It is evident that even with this reduced energy near complete ionization is achieved over most of the vapor column by the end of the laser pulse (30 ns).

In figure 9, the spatial variation of the electron temperature and the degree of ionization predicted to exist along the irradiated vapor column 10 ns from the start of the incident laser pulse for three values of laser detuning (0.14, 0.4 and 2.0 nm) are presented. Large gradients of both electron temperature and density are clearly predicted for laser detunings of 0.14 nm (or less). Indeed, it is expected that steep fronts of ionization and electron temperature propagate along the irradiated vapor column, especially for zero detuning of the laser.

Unfortunately, at about this time the laser had to be realigned after a component failure and this realignment caused the laser pulse to become slightly longer in duration (40 ns compared to 30 ns) and larger in cross section. The new empirical fit to the laser temporal profile was found to be given by

$$F(o, t) = F_p A t^B e^{-Ct^2} \qquad (29)$$

where $A = 3.352\times10^{-3}$, $B = 2.642$ and $C = 6.50\times10^{-3}$. The new cross sectional area was 0.236 cm^2 and the current relation between the peak photon flux density F_p and the laser energy fluence ε^{ℓ} is of the form

$$F_p \text{ (photons cm}^{-2} \text{ sec}^{-1}) \approx 2\times10^{23}\ \varepsilon^{\ell} \text{ (mJ cm}^{-2}) \qquad (30)$$

In order to model the three dimensional nature of this interaction we divided the lateral distribution of the laser pulse into several concentric annular shells and equated the laser energy fluence of each shell to the corresponding mean value in the radial distribution.

The interaction along the length of each shell was then computed. The lateral variation of electron density, electron temperature and laser irradiance could then be determined.

An example of the lateral distribution of electron density and electron temeprature predicted at the centre of the sodium vapor distribution for two instants of time is displayed in figure 10. In this instance the computer was simulating an experimental run in which the sodium atom density at the centre of the heat sandwich oven was measured to be 1.5×10^{16} cm^{-3} and the energy in the laser pulse was estimated to be 19.7 mJ with a burn spot average radius of 2.74 mm. For the computer run the incident laser pulse was assumed to have a Gaussian radial distribution with an exponential radius, r_o of 1.225 mm. The incident peak radial laser photon flux density F_p^{ℓ} distribution is also shown in figure 10.

It is apparent that the computer code predicts that near full ionization is achieved out to a radius of about 1.5 mm and that the electrons are hottest at the edge of the laser beam. The predicted cool annular region adjacent to the hot region is associated with a rapid ionization burnout occurring at 25 ns at that radial location. It should be mentioned that our assumption of a Maxwellian distribution for the free electrons is likely to break down for $N_e \lesssim 10^{15}$ cm^{-3} and so the reliability of our temperature predictions very close to the edge of the laser beam is questionable.

As indicated in the subsequent section we are on the verge of measuring the radial electron density and temperature profiles produced by laser resonance absorption. Consequently, as an initial test of the accuracy of our three dimensional modeling of this laser ionization technique we decided to compare the predicted temporal shape and energy fluence of the transmitted laser pulse with that observed in an experiment. From the many computer runs corresponding to various incident laser energy pulses we have drawn a curve of laser energy fluence absorbed (mJ cm^{-2}) against incident peak laser photon flux density F_p (or energy fluence) for the case of a peak sodium density of 1.5×10^{16} cm^{-3} and a laser detuned to lie halfway between the two resonance line wavelengths, i.e., λ^{ℓ} = 589.3 nm. This curve is presented as figure 11, and using it we can calculate the amount of laser energy transmitted in each of the annular shells. This

enables us to essentially predict the amount of energy transmitted through the above sodium atom distribution for any radial profile of incident laser energy of wavelength 589.3 nm.

To compute the temporal shape and energy of any given transmitted laser pulse we must reconstitute this laser pulse from the set of transmitted laser pulses that were used to represent the incident laser pulse. The results of our first such synthesis and the corresponding experimental data are presented in figure 12. It can be seen that the predicted transmitted laser pulse approximates quite well the experimentally monitored laser pulse propagating through the sodium vapor. This preliminary comparison gives us some degree of confidence in our three dimensional modeling of LIBORS.

New LIBORS Facility and Experiments

During the past year our laboratory has undergone a major reorganization centred about the installation of a new laser facility and an associated electronic data acquisition and reduction system. As stated in our previous technical report the Phase-R flashlamp pumped dye laser which had formed the workhorse of our initial LIBORS experimental program suffered several major failures and never met specifications.

At the heart of the new facility is a Nd-YAG HY750 oscillator/amplifier laser manufactured by J. K. Lasers of the U.K. and distributed on this continent by Lumonics. This system also includes second and third harmonic generators and its specifications are indicated in Table 2. The second part of this faclity is a Quanta-Ray (oscillator/amplifier) PDL-1 dye laser that is pumped by either the second or third harmonic of the Nd-YAG laser. We also have provision for frequency doubling the output of the dye laser or frequency mixing it with the fundamental of the Nd-YAG laser. An overview of this new laser facility is presented as figure 13, while a photograph of the laboratory is shown as figure 14. The Nd-YAG laser can be seen in the background. The sodium heat sandwich oven with its flexible tubing carrying the cooling water is clearly visible at the centre of the picture. The photodetection system, including the vertically mounted SPEX 1700II monochromator, a small Heath monochromator, various photodiodes and a camera, are also seen on the granite table.

Table 2

Nd-YAG Laser Facility Specifications

Nd-YAG		
Output energy	(at 1.06 μm)	850 mJ
	(at 532 nm)	320 mJ
	(at 355 nm)	220 mJ
FWHM pulse duration	(at 1.06 μm)	20 ns
	(at 532 nm)	17 ns
Repetition rate		10 Hz

In order to optimize the use of this versatile and powerful new laser facility we have also switched our mode of operation and data acquisition during this period. Originally we recorded single pulses on a fast oscilloscope using cameras, then manually digitized these photographs. With the purchase of an EGG (4420) signal averager we now acquire the photomultiplier signals electronically and perform data reduction by means of an Apple II Plus microcomputer that also serves as a terminal to the Institute's new Perkin Elmer 3250 computer. This reorganization of the laboratory has limited our experimental program during the first six months, but in the past six months we have completed several runs with this new facility.

An evaluation of the free electron temperature of the sodium plasma produced through laser resonance saturation constitutes one of the most important measurements to be undertaken. Initially the emission from a series of spectral lines was monitored and the spatially averaged electron temperature deduced. This measurement was undertaken by imaging a small portion of the interaction region onto the entrance slit of the vertically mounted SPEX monochromator, permitting a horizontal slice of the plasma about 5 mm long and 50 to 250 μm wide to be observed. A representative spectral scan of the sodium emission, extending from 626 nm to 452 nm, is presented as figure 15. A higher resolution spectral scan of the $4\,^2D$-$3\,^2P$ multiplet is displayed as figure 16. In a later experiment the focussing lens was adjusted so that the region of observation was scanned vertically allowing the lateral distribution of the emission to be observed.

Electron Temperature Measurements

The steady state solution to the one dimensional radiative transfer equation enables the spectral radiance $J_{nm}(\nu, \ell)$ arising from the n to m transition and emitted in the x-direction from a slab of plasma to be written in the form

$$J_{nm}(\nu, \ell) = \int_0^{\ell} \varepsilon_{nm}(\nu, x)\exp\left[-\int_0^{x} \{\varepsilon_{nm}(\nu, x^*)/P(\nu, x^*)\}dx^*\right]dx \qquad (31)$$

where

$$\varepsilon_{nm}(\nu, x) \equiv \frac{h\nu}{4\pi} N_n(x)A_{nm}L_{nm}(\nu, x) \qquad (32)$$

represents the volume emission coefficient with $N_n(x)$ the upper state population density at x, A_{nm} the Einstein spontaneous emission probability and $L_{nm}(\nu,x)$ is the associated line profile function at x. If the plasma is assumed to be in local thermodynamic equilibrium we may write

$$P(\nu, x) = \frac{2h\nu^3}{c^2}\left[\exp\{-h\nu/kT_e(x) - 1\}\right]^{-1} \qquad (33)$$

which is the Blackbody spectral radiance (or Planck function) with $h\nu$ as the nm transition photon energy and $T_e(x)$ the free electron temperature at x.

If the plasma is uniform equation (31) simplifies to the form

$$J_{nm}(\nu, \ell) = P(\nu, T_e)\left[1 - \exp\left\{-\frac{\varepsilon_{nm}(\nu)}{P(\nu, T_e)}\ell\right\}\right] \qquad (34)$$

The optical thickness of the plasma at this frequency,

$$\tau_{nm}(\nu, \ell) \equiv \frac{\varepsilon_{nm}(\nu)\ell}{P(\nu, T_e)} \tag{35}$$

If $\tau_{nm}(\nu, \ell) << 1$, so the plasma is optically thin, then

$$J_{nm}(\nu, \ell) \simeq \varepsilon_{nm}(\nu)\ell \tag{36}$$

or the radiance of this line

$$J_{nm}(\ell) \equiv \int J_{nm}(\nu, \ell)d\nu = \frac{h\nu}{4\pi} N_n A_{nm} \ell \tag{37}$$

In a plasma produced by laser resonance saturation, we can assume that the level populations are decribed by a Boltzmann distribution down to the p^{th}-level. Under these circumstances we can write

$$\ell n\left[\frac{J_{nm}(\ell)}{\nu_{nm} g_n A_{nm}}\right] = C - \frac{E_{np}}{kT_e} \tag{38}$$

where g_n is the degeneracy of the n^{th}-level and C is a number that is the same for any transition and is therefore not important. In the optically thin limit we can experimentally treat the multiplet as a single spectral line. If I_n represents the photodetector signal arising from the multiplet emission, then we can write

$$I_n = R_n T \sum J_{nm}(\ell) \tag{39}$$

where R_n depends on the transition and involves the spectral response of the photodetection system while T is a constant of proportionality that is common to all transitions provided the same photodetector is used. The sum in (39) includes all the lines of the multiplet and n is now taken to represent the multiplet. Consequently, if LTE is assumed to extend down to the resonance levels we can write

$$\ln[I_n K_n] = \text{constant} - E_{n2}/kT_e \qquad (40)$$

where

$$K_n \equiv (R_n \nu_{nm} g_n A_{nm})^{-1} \qquad (41)$$

Plotting the right hand side of equation (40) against E_{n2} for the 5s-3p, 4d-3p, 6s-3p, 5d-3p, 7s-3p and 6d-3p multiplets should give a straight line of slope $(-1/kT_e)$.

In figure 17, the small circles; (o) represent the results of one experimental run and the straight line is derived on the basis of a linear regression analysis. The slope of this line provides us with the apparent temperature, T_e = 4328K. The deviation of the experimental points from this straight line suggests a pattern with transitions originating on the s-levels lying above the line and transitions originating on d-levels lying below it. This scatter of the data strongly suggests that the plasma is not optically thin for spectral lines terminating on the $3^2P_{1/2,3/2}$ resonance levels.

If we can no longer assume that the plasma is optically thin then we must use equation (34) to define the spectral radiance at ν arising from the nm-transition. In the case of sodium the ^2S-^2P multiplets comprise two transitions, while the ^2D-^3P multiplets comprise three. If we assume that the spectral lines are primarily electron impact Stark broadened, then we can write

$$L_{nm}(\nu) = \frac{1}{\pi} \cdot \frac{\gamma_{nm}}{(\nu - \nu_{nm} - s_{nm})^2 + \gamma_{nm}^2} \qquad (42)$$

where γ_{nm} represents the frequency Stark HMHW and s_{nm} the Stark shift for the nm transition. Both are linearly proportional to the free electron density.[27]

It is evident from equations (32) and (34) that evaluation of the spectral radiance requires knowledge of the upper state number density. If

we assume a Boltzmann distribution down to the resonance level, laser saturation of the resonance transitions and continuity, we can write

$$N_2 = \frac{G(N_o - N_e)}{1 + \alpha G} \tag{43}$$

where N_o is the initial (prior to irradiation) sodium atom density, N_e is the free electron density,

$$G \equiv g_2/(g_2 + g_1) \tag{44}$$

and

$$\alpha \equiv \sum_i (g_i/g_2)\exp(-E_{i2}/kT_e) \tag{45}$$

represents the pseudo-partition function — based on the laser saturated resonance state acting as a pseudo-ground state divided by the g_2.

The spectral radiance at ν arising from the transitions that comprise the n-multiplet,

$$J_n(\nu, \ell) = P(\nu, T_e)\left[1-\exp\left\{-\frac{h\nu G(N_o-N_e)}{4\pi P(\nu, T_e)(1+\alpha G)g_2}\sum A_{nm}L_{nm}(\nu)g_n\exp(-E_{n2}/kT_e)\right\}\right] \tag{46}$$

where the sum in (46) extends over the transitions that constitute the n-multiplet. It is evident that $J_n(\nu, \ell)$ is a function of three independent variables: N_e, T_e and ℓ.

Equation (46) was solved by means of an iterative procedure that converged on the optimum values of (N_e, T_e and ℓ) for the set of experimentally measured emission lines. The small triangles in figure 17 represent the computed values, derived in this manner (but assuming $\alpha G \ll 1$), that best fit the experimental data. The corresonding one slab electron temperature is 2444K while the degree of ionization is 22.8%.

This low value for the electron temperature is much less than predicted by our LIBORS code. We feel that part of this difference may be the inadequacy of a one slab model in allowing for optical depth effects. Indeed, radiation trapping of the resonance radiation could create a substantial halo of resonance state atoms that lie beyond the ionized region and absorb the observed spectral lines.

In reality both the electron density and temperature will vary considerably across the plasma column created by the laser pulse. The radial distributions of both the electron density and the electron temperature can be evaluated by a much more elaborate series of measurements. This involves measuring the spectral emission at a number of locations across the radius of the plasma column.

The spectral radiance at frequency ν, arising from the nm-transition and observed in the x-direction at some height y above the axis of a cylindrical plasma column of radius R can be expressed in the form

$$J_{nm}(\nu,y) = \int_{-\sqrt{(R^2-y^2)}}^{\sqrt{(R^2-y^2)}} \varepsilon_{nm}(\nu,y,x)\exp\{-\int_{x}^{\sqrt{(R^2-y^2)}} \frac{\varepsilon_{nm}(\nu,y,x^*)dx^*}{P(\nu,y,x^*)}\}dx \qquad (47)$$

See the top left hand corner of figure 18.

If the plasma can be regarded as optically thin at this frequency and azimuthally symmetric we can spectrally integrate over the transitions of the n-multiplet and write

$$J_n(y) = 2\int_{0}^{\sqrt{(R^2-y^2)}} \varepsilon_n(y,x)dx \qquad (48)$$

for the radiance observed in the x-direction at height y and arising from the emission in the n-multiplet, where

$$\varepsilon_n(y,x) = \sum \varepsilon_{nm}(y,x) \qquad (49)$$

The sum extending over the transitions that comprise the n-multiplet. Alternatively we can write

$$J_n(y) = 2 \int_o^R \frac{\varepsilon_n(r) r dr}{\sqrt{(r^2 - y^2)}} \qquad (50)$$

by introducing $r^2 = x^2 + y^2$, which can be inverted, using the Abel transform to provide the radial distribution of volume emission coefficient,

$$\varepsilon_n(r) = -\frac{1}{\pi} \int_r^R \left\{\frac{dJ_n(y)}{dy}\right\} \cdot \frac{dy}{\sqrt{(y^2 - r^2)}} \qquad (50)$$

As indicated earlier we can relate $J_n(y)$ to the corresponding photodetector signal $I_n(y)$ through the relation

$$I_n(y) = R_n T J_n(y) \qquad (51)$$

This enables us to determine the radial distribution of emission on the n-multiplet in terms of the measured signal variation across the plasma column, that is to say,

$$\varepsilon_n(r) = -\frac{1}{\pi R_n T} \int_r^R \left\{\frac{dI_n(y)}{dy}\right\} \cdot \frac{dy}{\sqrt{(y^2 - r^2)}} \qquad (52)$$

If we then compare the volume emission from two multiplets (n and q) — in practice the 6^2D-3^2P and 4^2D-3^2P of sodium, then we can write

$$\frac{\varepsilon_n(r)}{\varepsilon_q(r)} = \frac{R_q}{R_n} \frac{\int_r^R \left\{\frac{dI_n(y)}{dy}\right\} \frac{dy}{\sqrt{(r^2-y^2)}}}{\int_r^R \left\{\frac{dI_q(y)}{dy}\right\} \frac{dy}{\sqrt{(r^2-y^2)}}} = S_{nq}(r) \qquad (53)$$

However,

$$\frac{\varepsilon_n(r)}{\varepsilon_q(r)} = \frac{\sum \nu_{nm} N_n(r) A_{nm}}{\sum \nu_{qp} N_q(r) A_{qp}} = B_{nq} \exp\{-E_{nq}/kT_e(r)\} \qquad (54)$$

where B_{nq} is a constant that depends on the atomic parameters of the two multiplets. Consequently, the radial electron temperature profile

$$T_e(r) = - \frac{E_{nq}/k}{\ln\{B_{nq}/S_{nq}(r)\}} \qquad (55)$$

can be evaluated.

In figure 18 the observed distribution of signals for both the $6\,^2D$-$3\,^2P$ and $4\,^2D$-$3\,^2P$ multiplets across the plasma column are presented for an experiment in which the laser was tuned to the $3\,^2S_{1/2}$-$3\,^2P_{3/2}$ transition at 589.0 nm, the incident energy was 37 mJ and the peak sodium atom density was estimated to be around 1.5×10^{16} cm^{-3}. The magnification of the optics was 1:1, with the SPEX monochromator entrance slit set at 1 cm × 40 μm. The signal from the RCA 7265 photomultiplier tube was processed by the EGG signal averager gated such that it sampled the emission in a 2 ns interval, approximately 60 ns after the onset of the incident laser pulse. Since the laser pulse duration was under 40 ns, the influence of the laser field (through the dynamic Stark effect) should be minimal and spontaneous decay of the resonance state population should minimize optical depth effects

(unfortunately all of the lines accessible with our present photomultiplier terminate on one of the resonance levels).

The curves drawn through the experimental points represent a least square fit using a polynomial of the form

$$Q(y) = \{C_1 + C_2y^2 + C_4y^4\}\exp(-C_5y^2) \qquad (56)$$

where the fitting parameters C_1, C_2, C_4 and C_5 are chosen to minimize the residual sum of the squares of the deviations from the actual data points. The Abel inversion of these polynomials is then possible and the ratio of the inverted curves is used to estimate the radial electron temperature distribution. The experimental data presented in figure 18 gives rise to the radial electron temperature profile shown in figure 19. Three theoretical temperature profiles associated with three very different laser radial distributions are also displayed in figure 19. Each was synthesised from a series of LIBORS computer runs of different incident laser irradiance as discussed earlier. The sharp temperature peaks predicted for two of the cases are very unlikely to occur in reality due to thermal conduction. As indicated earlier we are presently working on a new code that will allow for thermal conduction. Although this will invariably smooth out the temperture profile - there remains an important difference in the magnitude of the temperature predicted by our code and that determined experimentally. Currently we are exploring several possible explanations for this difference.

It should be noted that there is reasonable agreement between the spatially averaged experimentally measured T_e of figure 19 and the "apparent" T_e determined from the Boltzmann plot for the six spectral lines, see figure 17. As indicated earlier it is quite likely that the optical depth of the plasma could be significant for transitions terminating on the resonance levels. This will require correcting this temperature profile for optical depth effects.

To accomplish this we plan to determine the radial electron density profile by deconvoluting the Stark broadened spectra of the 4^2D-3^2P multiplet. Then knowing N_o and assuming LTE we can estimate the radial resonance state distribution and correct both N_e and T_e measurements for self-absorption by an iterative procedure.

Spectral scans of the 4^2D-3^2P multiplet were taken for 15 positions across the plasma column. The spectral resolution was estimated to be 0.05 nm (FWHW) with 16 laser shots being averaged to constitute one measurement and 128 such measurements comprising one spectral scan. Two representative spectral scans of the 4^2D-3^2P multiplet are presented as figure 20. The emission originating from the central core of the plasma (y = 0.25 mm) is seen to suffer a much greater Stark broadening (and red shift) than the emission arising from the more weakly ionized rim of the plasma column (y = 2.25 mm). The laser in this run was tuned to the 589.0 nm sodium resonance line with an energy of about 37 mJ. As before the time of observation was 60 ns from the start of the laser pulse and the peak sodium atom density was determined to be about 1.5×10^{16} cm^{-3}.

At the present time we are developing a computer code to perform the deconvolution of this spectral information. Generalization of equation (52) leads to

$$\varepsilon_n(\nu, r) = -\frac{1}{\pi R_n T} \int_r^R \left\{\frac{dI_n(\nu, y)}{dy}\right\} \frac{dy}{\sqrt{(y^2-r^2)}} \qquad (57)$$

Since $L_n(\nu, r)$ is proportional to $\varepsilon_n(\nu, r)$ we can use Stark broadening to evaluate $N_e(r)$ given an approximate value for $T_e(r)$. An optical depth correction will be undertaken along the lines discussed earlier for the case of the electron temperature profile.

Alternatively, it is possible to consider using emission on either the sodium 6^2P-4^2S or 7^2P-4^2S multiplets as these should not be optically thick. To accomplish this we would have to use an RCA 31034 photomultiplier which as a GaAs photocathode and a reasonable spectral response to about 850 nm. Unfortunately, this photomultip lier has to be cooled with a carefully controlled system to maintain a constant sensitivity. Currently, we are in the process of acquiring such a system and plan to compare the electron density and temperature profiles evaluted in this manner with those determined using the optical depth correction procedure.

Laser Off-Resonance Maximum Absorption (LORMA)-Effect

During the past year we have undertaken an investigation of the sensitivity of laser ionization based on resonance saturation to the spectral detuning of the laser and have made a surprising experimental observation. Under certain conditions it appears that maximum absorption of the laser pulse arises when the laser is detuned by about 0.4 to 0.5 nm to either the blue of the 589.0 nm or red of the 589.6 nm sodium resonance lines. This minimum in the transmitted energy has been observed with both the long pulse (1 μsec) from our old flashlamp pumped dye laser and the short pulse (30 ns) from our new Nd-YAG laser pumped dye laser.

This laser off-resonance maximum absorption (LORMA)-effect is most pronounced at higher densities. An example is provided by figure 21 where a distinct minimum in the transmitted laser energy is seen to occur at about 0.4 nm to the blue of the 589.0 resonance line (marked as 0 on wavelength scale). The peak sodium atom density in this run was estimated to be about 4×10^{16} cm^{-3}. It is also apparent that very strong attenuation arises between the resonance lines and that there might also be a local minimum at the line centre wavelength. However, more recent low density runs have not substantiated this latter observation and have suggested that there might even be an asymmetry in the strength of the LORMA effect, with more attenuation occurring on the red side of the 589.6 nm resonance line.

Simulation of this LORMA-effect we felt would constitute a good test of our new LIBORS computer code. The results of three such detuning computer runs for $F_p = 3.75\times10^{25}$ photons cm^{-2} sec^{-1} (27 mJ), 2.625×10^{25} (19 mJ) and 2.25×10^{25} (11 mJ) are presented as figure 22. The peak sodium atom density was taken to be 4×10^{16} cm^{-3} to correspond to the experimental conditions that applied to figure 21. It is immediately evident that a well defined minimum in the transmitted laser energy is predicted to arise for a laser detuning of around 0.4 to 0.5 nm. It should be noted, however, that no computer runs with $\Delta\lambda_\ell < 0.14$ nm were undertaken due to the strong laser coupling and the subsequent large increase in computational time accompanying these small values of laser detuning. Nevertheless, it is obvious that our new LIBORS computer code predicts this LORMA-effect.

The physical mechanism responsible for this effect can be understood if we recall that the dominant photon loss process is absorption by the resonance transition and that once the free electron density exceeds about

10^{15} cm^{-3} a dynamic balance is established between the rate of laser absorption and the rate of superelastic electron quenching of the laser pumped resonance state population, see figure 1. This suggests that the rate of laser energy absorption will be proportional to the product of the resonance state population and the free electron density.

We propose that the explanation of this LORMA-effect lies in the fact that a slightly detuned ($\Delta\lambda_\ell \simeq 0.4$ nm) laser pulse still produces close to full ionization, albeit with a much longer ionization time. As a consequence the product of the resonance state population with the free electron density remains large for an extended period of time and this maximizes the energy extracted from the laser pulse by electron superelastic collisions. In other words when the laser is sharply tuned to a resonance line the ionization proceeds so fast that the sodium superelastic electron laser energy converters, see figure 1, cannot go through many cycles before they are destroyed by ionization. On the other hand when the laser is detuned far from the resonance line the degree of ionization never gets very large and laser saturation may break down reducing, in effect, both the free electron density and the resonance state population density.

It is clear that there exists some intermediate detuning of the laser for which the number of absorption-superelastic collision cycles is a maximum. This constitutes the detuning that extracts the maximum energy from the laser pulse. A more detailed analysis is provided in Appendix A. We may therefore conclude that this new observation represents further evidence of the primary role played by superelastic electron collisions in extracting energy from the laser pulse.

An interesting question is raised by the LORMA-effect: if more energy is extracted from a laser pulse that is detuned by 0.4 nm compared to one tuned close to the resonance line - should this additional energy not appear in the radiation emitted by the resulting plasma? In figure 23 we provide evidence of just such an observation taken some time ago with our old flashlamp pumped dye laser. The upper trace of figure 23(a) displays the incident laser pulse photodiode signal while the lower trace provides the recombination radiation in a 5.0 nm band centred about 405 nm and detected by a photodetection system comprising a JY-monochromator and an RCA 1P28 photomultiplier. In this experiment the laser was tuned to the

589.6 nm resonance line of sodium, while in figure 23(b) the same information is displayed but for a laser pulse that is detuned to 590.1 nm.

It is quite clear from figure 23 that the amount of radiative recombination emitted when the laser is detuned by 0.5 nm is greater than when it is tuned to the 589.6 nm resonance line. Close inspection of this figure also reveals another important difference that is in keeping with our theoretical results - there is virtually no delay between the onset of recombination radiation for the detuned laser while there is a substantial delay in the case of the tuned laser pulse.

Thermal Conduction and LIBORS

Our attempts at modeling the three dimensional nature of LIBORS have revealed that strong electron temperature gradients would tend to develop, see for example figures 9, 10 and 19. In reality the tendency to produce strong electron temperature gradients would be countered by electron energy transport through thermal conduction. Our theoretical treatment to date has omitted thermal conduction. The justification for this omission is open to question in light of our recent findings.

If we take electron thermal conduction into account equation (14), which describes conservation of electron energy, is modified and takes the form

$$\frac{\partial u_e}{\partial t} + \nabla \cdot \underset{\sim}{q}_e = C_e^{\text{LIBORS}} \tag{58}$$

where $u_e = \int \frac{1}{2} m_e v^2 f(v) d^3v$ represents the electron kinetic energy density, $\underset{\sim}{q}_e = \int \frac{1}{2} m_e v^2 \underset{\sim}{v} f(v) d^3v$ represents the electron kinetic energy flow vector and C_e^{LIBORS} stands for all of the collisional energy sources and sinks previously introduced on the right hand side of equation (14). It should be noted that the form of equation (58) assumes that Joule heating is negligible. In the absence of an applied electric field this assumption is

reasonable due to ambipolar effects.[28] The same reasoning permits us to write,

$$\underset{\sim}{q}_e = -\lambda \nabla T_e \tag{59}$$

where λ represents the electron thermal transport coefficient.

If the energy flow is not excessive the electron velocity distribution, $f(v)$, will not deviate too greatly from the equilibrium electron velocity distribution, $f_0(v)$, and we can express it in the form of the truncated expansion,

$$f(v) = f_0(v) + \underset{\sim}{f}_1(v) \cdot \underset{\sim}{v}/v \tag{60}$$

If this is used in the Boltzmann equation for the electrons and the resultant equation divided into two differential equations, one of them takes the form

$$\frac{\partial \underset{\sim}{f}_1(v)}{\partial t} + \underset{\sim}{v} \cdot \nabla f_0(v) - \frac{e\underset{\sim}{E}}{m_e} \cdot \frac{\partial f_0(v)}{\partial v} = -\nu_{eff}(v)\underset{\sim}{f}_1(v) \tag{61}$$

where m_e is the mass of the electron and $\underset{\sim}{E}$ represents the electric field. The right hand side of equation (61) arises from a "Mixture Rule",[28] where ν_{eff} represents an effective momentum exchange collision frequency that accounts for all forms of elastic collisions between the electrons and the heavy species such as sodium atoms, argon atoms and sodium ions.

Now in general the collision time is considerably shorter than the typical time for a significant change in the velocity distribution and consequently we may write

$$\underset{\sim}{f}_1(v) \simeq -\frac{v}{\nu_{eff}} \nabla f_0(v) + \frac{e\underset{\sim}{E}}{m_e \nu_{eff}} \frac{\partial f_0(v)}{\partial v} \tag{62}$$

If $f_0(v)$ is Maxwellian, i.e.,

$$f_0(v) = \left(\frac{m_e}{2\pi k T_e}\right)^{3/2} \exp\left\{-\frac{m_e v^2}{2kT_e}\right\} \tag{63}$$

then equation (62) can be expressed in the form

$$\underset{\sim}{f}_1(v) = -\frac{ev}{kT_e \nu_{eff}} f_0(v)\left\{\underset{\sim}{E} + \frac{\nabla p_e}{eN_e}\right\} - \left\{\frac{m_e v^2}{2kT_e} - \frac{5}{2}\right\} \frac{v}{\nu_{eff}} f_0(v) \frac{\nabla T_e}{T_e} \tag{64}$$

If we use equation (60) for f(v) in the definition of $\underset{\sim}{q}_e$ we arrive at the expression

$$\underset{\sim}{q}_e = \frac{2\pi m_e}{3} \int_0^\infty v^5 \underset{\sim}{f}_1(v) dv \tag{65}$$

which can be rewritten in the form

$$\underset{\sim}{q}_e = -\frac{5}{2}\frac{kT_e}{e} \underset{\sim}{j}_e + \frac{2\pi m_e}{3} \int_0^\infty v^3 \underset{\sim}{f}_1(v) dv \tag{66}$$

where the electron current density

$$\underset{\sim}{j}_e = -\frac{2\pi e}{3} \int_0^\infty v^3 \underset{\sim}{f}_1(v) dv \tag{67}$$

using the same assumptions as above.

Substitution of equation (64) into (66) yields

$$\underset{\sim}{q}_e = -\frac{5}{2} kT_e \underset{\sim}{j}_e - \lambda^* \nabla T_e - T_e \phi \{\underset{\sim}{E} + \frac{\nabla p_e}{eN_e}\} \tag{68}$$

However, it can be shown[28] that

$$\underset{\sim}{E} + \frac{\nabla p_e}{eN_e} = \frac{1}{\sigma} \{\underset{\sim}{j}_e - \phi \nabla T_e\} \tag{69}$$

which enables us to write

$$\underset{\sim}{q}_e = \psi \underset{\sim}{j}_e - \lambda \nabla T_e \tag{70}$$

where

$$\psi = -\frac{5kT_e}{2e} - \frac{T_e \phi}{\sigma} \tag{71}$$

$$\lambda = \lambda^* - \frac{T_e \phi^2}{\sigma} \tag{72}$$

$$\phi = \frac{4\pi e}{3T_e} \int_0^\infty \frac{1}{\phi \nu_{eff}} \{\frac{m_e v^2}{2kT_e} - \frac{5}{2}\} v^4 f_0(v) dv \tag{73}$$

$$\sigma = \frac{4\pi e^2}{3kT_e} \int_0^\infty \frac{1}{\sigma \nu_{eff}} v^4 f_0(v) dv \tag{74}$$

$$\lambda^* = \frac{4\pi k}{3} \int_0^\infty \frac{1}{\lambda \nu_{eff}} \left\{\frac{m_e v^2}{2kT_e} - \frac{5}{2}\right\}^2 v^4 f_0(v) dv \qquad (75)$$

and

$$\nu_{eff}^{\lambda,\sigma,\phi} = \sum_n \nu_{en} + A^{\lambda,\sigma,\phi} \frac{8\pi N_i}{v^2} \left(\frac{m_e}{2kT_e}\right)^{1/2} \left(\frac{e^2}{4\pi\varepsilon_o m_e}\right)^2 \ell n \Lambda \qquad (76)$$

with $A^\lambda = 1.012$, $A^\sigma = 0.476$ and $A^\phi = 0.6776$. $\ell n \Lambda$ is the usual Coulomb logarithm.

The first term on the right hand side of equation (76) represents the sum of the electron momentum transfer collision frequencies for each of the sodium atomic states (primarily ground and resonance state atoms) and the argon atoms, while the second term represents the electron-ion momentum transfer collision frequency. The three different coefficients A^λ, A^σ and A^ϕ are required in order that the expressions used agree in both the low and high ionization limit with those obtained when electron-electron collisions are rigourously included.[28]

If the plasma is fully ionized then the first term on the right hand side of equation (76), representing the sum of collision frequencies involving neutral atoms, is zero and λ becomes the Spitzer-Harm value, λ_{SH}. Ambipolar effects are found to make the first term on the right hand side of (70) negligible compared to the second, so that we usually write

$$\underset{\sim}{q}_e = -\lambda \nabla T_e \qquad (77)$$

It should be noted that λ is in general smaller than λ_{SH} and it therefore follows that electron thermal conduction for a partially ionized vapor is less than for a fully ionized vapor.

For the case of a sodium plasma formed by laser resonance saturation the ratio of λ/λ_{SH} has been computed for an original sodium density (prior to laser excitation) of 10^{16} cm^{-3} as a function of the free electron temperature. The results are presented in figure 24.

The full curve (——) corresponds to the case where LTE is assumed down to the resonance state as the resonance transition is laser saturated, while the broken curve (— — —) corresponds to LTE down to the ground state. Also displayed by the dotted curve (••••••) in figure 24 is the

variation of λ/λ_{SH} with T_e for the situation where argon at a density of 5×10^{16} cm $^{-3}$ is added to the first case. The variation of λ_{SH} with electron temperature is also provided by the (—Δ—) curve in figure 24.

These results clearly indicate that the Spitzer-Harm electron thermal conductivity λ_{SH} is reliable to within 15% of the exact value for electron temperatures greater than 4000 K, irrespective of the model used. For electron temperatures less than this value the thermal conductivity rapidly drops and we could probably ignore electron thermal conduction.

Self-Pumped Resonance Inversion Scheme

An intense flash of light was used to excite the first laser and many of today's most popular lasers involve optical pumping. In the race to develop an X-ray laser, radiative pumping schemes figure prominently.[29-34] In almost all of these a coincidence is sought between the wavelength emitted by the radiating ion species and that absorbed by the recipient ion species.[34]

In this section we consider a new approach towards the development of short wavelength (EUV to X-ray) lasers based on sudden radiative pumping. The central feature of this "self-pumped resonance inversion" (SPRI)-scheme is the large fine structure splitting of the ground state found in members of the thallium (and to a lesser extent in the indium-)-isoelectronic series.

In order to explain the SPRI-scheme we shall consider a representative example of the Tℓ-isoelectronic series...doubly ionized bismuth. A partial Grotrian energy level diagram of the lowest BiIII levels is presented as figure 25. If a plasma containing BiIII as a major constituent is suddenly heated a burst of emission on all the strong lines will ensue. If this radiation is directed at a cold BiIII plasma photoexcitation from the $6^2P_{1/2}$ ground level will rapidly populate many of the higher levels, including the $7^2S_{1/2}$ and $6^2D_{3/2}$ levels. The upper level of the split ground state, $6^2P_{3/2}$, will not, however, be excited in this manner and this suggests that it may be possible to create a transient population inversion between the $6^2D_{3/2}$ (or to a lesser extent the $7^2S_{1/2}$) and $6^2P_{3/2}$ levels. This concept is schematically illustrated in figure 26.

Clearly, the larger the population initially residing in the $6^2P_{3/2}$ level the more difficult it will be to create the population inversion.

This tends to impose a restriction on the cold plasma temperature for a given source radiance or, equivalently, the minimum jump in the temperature of the radiating plasma.

Although there are many ways to rapidly heat a plasma, the temperature achieved is usually not controlled and uniformity rarely attained. Laser saturation of a low lying resonance transition of an ion that forms a major constituent of a plasma does, however, offer just these features[35] by way of superelastic electron heating.

The controlled jump in the electron temperature predicted for this superelastic heating technique is a direct result of the self-limiting nature of the interaction. In essence, once laser saturation of the resonance transition is achieved, the electron temperature is determined by a dynamic balance of superelastic and inelastic collisional processes and is therefore independent of the laser irradiance or even the density of the relevant ion. Such a controlled jump in the free electron temperature is important from both the standpoints of efficiency and optimization of the spectral composition of the emitted radiation.

In general, the radiating ion used in the SPRI-laser scheme will not be suitable for superelastic electron heating and as a consequence the hot plasma emission source will probably have to comprise both kinds of ions: those involved in heating the free electrons and those that emit the appropriate line radiation for pumping the cold plasma.

In our preliminary discussion of the self-pumping resonance inversion scheme we used the model indicated in figure 26. In essence a plasma comprising doubly ionized bismuth (BiIII) was assumed to be suddenly heated such that the free electron temperature jumped to a value T_e^H in a time that is short compared to times of interest. A subsequent step-like pulse of 104 nm line radiation, corresponding to the ($6^2D_{3/2} - 6^2P_{1/2}$) transition (see figure 25) would be emitted. This flash of radiation would propagate into the cold low density plasma of BiIII and serves to excite the $6^2D_{3/2}$ level of the recipient ion. Since there would be no corresponding excitation of the upper level of the split ground state, $6^2P_{3/2}$, we showed that a population inversion was created between levels $6^2D_{3/2}$ and $6^2P_{3/2}$, given a small enough initial population on the $6^2P_{3/2}$ level.

In this analysis we neglected the ($7^2S - 6^2P$) multiplet (see figure

25) as these transitions are somewhat weaker and we also neglected the effect of radiation at 122.5 nm corresponding to the ($6^2P_{3/2}$ - $6^2D_{5/2}$) transition. We further assumed that: the density in the cold plasma was low enough that collisional mixing and broadening could be neglected, while that of the hot plasma was adequate to ensure near blackbody emission on the lines of interest.

Under these circumstances we were able to show that a population inversion could be created for a hot plasma temperature of 9 eV and a cold plasma temperature of 1 eV. In the case of a cold plasma density of 10^{14} cm^{-3} a peak inversion density of several percent was predicted to arise on the 132.7 nm transition within a distance of 2×10^{-2} cm of the sharp boundary, see figure 27. This small gain region is a direct result of the short optical path of the 104 nm pump radiation and this has prompted us to consider if it would not be more fruitful to consider the population inversion that would be created on the 134.6 nm ($7^2S_{1/2}$ - $6^2P_{3/2}$) line through pumping on the weaker 105.2 nm line.

Within the past few months we have undertaken a more thorough analysis of this concept. This treatment takes account of all of the radiative processes coupling the 7^2S, 6^2D and 6^2P terms of BiIII and involves solving the following set of population rate equations:

$$\frac{dN_n}{dt} = \sum_{m<n} N_m R_{mn} + \sum_{s>n} N_s (R_{sn} + A_{sn}) - N_n \{ \sum_{m<n} (R_{nm} + A_{nm}) + \sum_{s>n} R_{ns} \} \quad (78)$$

for the five levels indicated in figure 25.

If we neglect higher states of excitation then continuity can be expressed by the relation

$$\sum_{1}^{5} N_n = N_o \quad (79)$$

where N_0 represents the initial BiIII ion ground state density, prior to irradiation. A further simplification is afforded by assuming that the population of levels 4 and 5 are always in the ratio of their degeneracies — this should be a conservative assumption. These two assumptions enable the set of five differential equations indicated by equation (78) to be reduced to three population equations.

If the cold BiIII plasma is assumed to be suddenly irradiated by blackbody radiation at temperature T_e^H, then the coefficients in the population rate equations are constants and solutions can be obtained directly. Since we are assuming that the density of the plasma is sufficiently low (10^{14} cm^{-3}) that collisional effects are negligible on the time scales of interest — we shall consider the lines to be Doppler broadened.

This more complete analysis reveals that no population inversion is created on either the $7^2S_{1/2}$ - $6^2P_{3/2}$ or $67^2D_{3/2}$ - $6^2P_{3/2}$ transitions for the hot and cold plasma temperatures of 9 eV and 1 eV, respectively. It should be noted that the temperature of the cold plasma only enters in determining the initial population of the $6^2P_{3/2}$ terminal level and the 1 eV was felt to be the minimum that would make sense for a BiIII plasma that was created sometime before irradiation. If, however, the BiIII plasma was generated very rapidly just prior to irradiation (maybe through multiphoton ionization) it may be possible to have a low $6^2P_{3/2}$ level population — equivalent to a 0.25 eV Boltzmann distribution. We have found that under these circumstances a population inversion of 0.5% and 1.2% can be created on the $6^2D_{3/2}$ - $6^2P_{3/2}$ and $7^2S_{1/2}$ - $6^2P_{3/2}$ transitions, respectively. It should also be noted that our assumption concerning the coupling of the populations on the $6^2D_{5/2}$ and $6^2D_{3/2}$ levels may be too conservative since the collisional relaxation time is likely to be much greater than the times of interest. If we decoupled these two levels we would probably obtain inversions for somewhat higher effective temperatures of the cold plasma.

New Three Photon Saturation Laser Scheme

During the past six months we have been studying the feasibility of a new approach towards the development of a short wavelength laser that is based on three photon saturation of an ion possessing a low lying

metastable state. The basic inversion scheme for the case of singly ionized strontium SrII is indicated in figure 28. In essence we propose that a momentary population inversion should be created between the 5^2F and 4^2D terms if the former is directly populated from the ground state by a three photon process while the latter is minimally excited.

The key to this concept is the rapid formation of the SrII ground state ions through two photon ionization of strontium vapor, and the simultaneous three photon excitation of the 5^2F term by the same laser field. This should provide a means of populating the 5^2F term before any appreciable population is produced on the 4^2D metastable term. The wavelength of the radiation (422 nm) required for this scheme is close to the resonance radiation of the SrII ion and as a consequence the three photon excitation cross-section should be considerably enhanced by this near resonance condition. Furthermore, the presence of the 5^2D term should also improve the strength of this interaction. If this concept is successful it could lead to an effective method of obtaining laser radiation at close to the third harmonic of the pump laser wavelength — but with much higher efficiency than can be achieved through present methods of third harmonic generation. It could also be extended to other wavelengths by using different transitions and other ions possessing low lying metastable states.

In order to test the feasibility of this method of creating a short wavelength laser we have initiated a combined theoretical and experimental program. These programs are designed to answer three important questions. First can we two photon ionize a reasonable length of strontium vapor with our Nd-YAG laser pumped dye laser, secondly can we excite a sufficient number of the SrII ground state ions into the 5^2F term to create a population inversion between 5^2F and 4^2D terms and thirdly is competition from either of the other 5^2F-n^2D ($n = 6$ or 5) multiplets likely to prevent laser action on the 5^2F-4^2D multiplet at 177 nm.

Theoretical Program

We have modeled the SrII ion by the 5-level system shown as figure 29. It is evident that laser radiation at about 422 nm can populate level 5 (corresponding to the 5^2F term of SrII) through three photon near resonant absorption. If the ions are created cold in the ground state at virtually

the same moment via two photon ionization of strontium vapor by the same laser pulse then clearly a population inversion would be created on the 5-4 and 5-3 transitions in addition to the desired inversion on the 5-2 transition.

The rate of three photon excitation can according to Yariv[36] be written in the form

$$W_p = \frac{27\pi e^6 I_L^{\,3}}{32(m_e \varepsilon_o c\hbar)^3} \; \frac{g_{15} f_{1r} f_{r3} f_{35}}{\omega_{r1}\omega_{r3}\omega_{53}(\omega_{r1}-\omega_L)^2(\omega_{31}-2\omega_L)^2\Delta\omega_{51}} \qquad (80)$$

where f_{mn} represents the absorption oscillator strength of the n-m transition and ω_{nm} the corresponding angular frequency. The resonance and intermediate levels involved in the three photon process are designated "r" and "3" respectively. $\Delta\omega_{51}$ represents the bandwidth and g_{15} the degeneracy ratio (g_1/g_5) of the 5-1 transition. I_L is the laser irradiance and the other constants have their usual values.

In reality there are several three photon paths that would lead to excitation of the 5^2F term:

(i) $5^2S_{1/2} \rightarrow 5^2P_{1/2} \rightarrow 5^2D_{3/2} \rightarrow 5^2F_{5/2}$

(ii) $5^2S_{1/2} \rightarrow 5^2P_{3/2} \rightarrow 5^2D_{3/2} \rightarrow 5^2F_{5/2}$

(iii) $5^2S_{1/2} \rightarrow 5^2P_{3/2} \rightarrow 5^2D_{5/2} \rightarrow 5^2F_{5/2}$

(iv) $5^2S_{1/2} \rightarrow 5^2P_{3/2} \rightarrow 5^2D_{5/2} \rightarrow 5^2F_{7/2}$

If the laser wavelength is tuned such that three photons just excite the 5^2F term (i.e., λ_L = 422.14 nm) then the near resonance with the $5^2S_{1/2}$-$5^2P_{1/2}$ transition (at 421.67 nm) ensures that we need only consider the first path as its rate will exceed the rates associated with the other paths by nearly two orders of magnitude due to the small value of the $(\omega_{r1}-\omega_L)$ factor in equation (80).

Under these circumstances the three photon excitation rate per ion

$$W_p(t) \simeq 1.96\times10^{-18} \frac{I_L{}^3(t)}{\Delta\omega_{51}} \tag{81}$$

where $I_L(t)$ is the laser irradiance at time t and $\Delta\omega_{51}$ is the bandwidth of the three photon transition. The appropriate population rate equations for our 5-level model are:

$$\frac{dN_5}{dt} = N_1W_p - N_{54}R_{54} - N_{53}R_{53} - N_{52}R_{52} - N_5A_5 \tag{82}$$

and

$$\frac{dN_n}{dt} = N_{5n}R_{5n} + N_5A_{5n} - N_nA_n \tag{83}$$

where n = 4, 3 and 2. In general, N_m is the population density of the m^{th} level, and $N_{nm} \equiv N_n - g_{nm}N_m$ represents the population inversion density between levels n and m. The stimulated emission rate

$$R_{5n} \equiv \frac{B_{5n}}{4\pi} \int I_{5n}(\nu)L_{5n}(\nu)d\nu \tag{84}$$

where B_{5n} represents the Milne stimulated emission coefficient, $L_{5n}(\nu)$ the line profile function and $I_{5n}(\nu)$ the spectral irradiance that arises from the 5-n transition. The total rate of spontaneous decay of level n,

$$A_n \equiv \sum_{m<n} A_{nm} \tag{85}$$

where the sum extends over all levels m lower than n.

If we assume that the radiation field originating from stimulated emission on the 5-n transition (where n = 4, 3 and 2) is much narrower than the appropriate atomic linewidth and centred at the appropriate line centre frequency, ν_{5n}, then we can write

$$I_{5n}(\nu) = I_{5n}\delta(\nu - \nu_{5n}) \tag{86}$$

where I_{5n} is the irradiance of the radiation field and $\delta(\nu - \nu_{5n})$ the appropriate delta function. Under these conditions

$$R_{5n} = \frac{B_{5n}}{4\pi} I_{5n} L_{5n} \tag{87}$$

where L_{5n} represents the value of the line profile function at the line centre frequency ν_{5n}.

In order to calculate the irradiance produced on each of the inverted transitions along the path of the pump beam we must obviously solve the above set of rate equations combined with the appropriate radiative transfer equations. In the first place we must take account of the attenuation of the pump laser pulse. Since the speed of light can be regarded as effectively infinite for our conditions and the laser beam is assumed to propagate primarily in the z-direction we can write

$$\frac{\partial I_L(z,t)}{\partial z} = -N_1(z,t)\beta I_L{}^3(z,t) - \{N_o - N_1(z,t)\}\alpha I_L{}^2(z,t) \tag{88}$$

where β represents the three photon excitation rate $\{\frac{1.96\times10^{-18}}{\Delta\omega_{51}}\} \times 3h\nu_L$, α the two photon ionization rate $\times 2h\nu_L$, N_o the strontium atom density prior to laser irradiation, $N_1(z,t)$ the strontium ion ground state density, and $I_L(z,t)$ the pump laser irradiance. $h\nu_L$ represents the laser photon

energy. Equation (88) has to be solved in conjunction with the ion creation equation:

$$\frac{\partial N_1(z,t)}{\partial t} = - \frac{\alpha I_L{}^2(z,t)}{2h\nu_L} \{N_0 - N_1(z,t)\} \qquad (89)$$

We shall now consider the growth of the radiation field on each of the 5-4, 5-3 and 5-2 transitions. To describe the amplification of the radiation field on the 5-n transition propagating in the z-direction we again use the steady state one dimensional radiative transfer equation — which in this instance takes the form

$$\frac{\partial}{\partial z} \{I_{5n}(\nu,z)\} = h\nu_{5n} A_{5n} N_5 L_{5n}(\nu) \frac{\Delta\Omega}{4\pi} + \sigma_{5n}(\nu) N_{5n} I_{5n}(\nu,z) \qquad (90)$$

where $I_{5n}(\nu,z)$ represents the spectral irradiance at z arising from the 5-n transition and $\sigma_{5n}(\nu)\{\equiv \frac{h\nu_{5n}}{4\pi} B_{5n} L_{5n}(\nu)\}$ represents the corresponding stimulated emission cross section with n = 4, 3 and 2.

If we integrate over a range of frequencies that sufficiently encompass the 5-n line and takes account of our assumption regarding the narrow bandwidth of the emission we can write

$$\frac{dI_{5n}(z)}{dz} = \varepsilon_{5n} \Delta\Omega + \alpha_{5n} I_{5n}(z) \qquad (91)$$

where ε_{5n} $\{\equiv \frac{h\nu_{5n}}{4\pi} N_5 A_{5n}\}$ is the spectrally integrated volume spontaneous emission coefficient, $I_{5n}(z)$ is the irradiance of the radiation at position z and

$$\alpha_{5n} = \frac{h\nu_{5n}}{4\pi} B_{5n} L_{5n} N_{5n} \qquad (92)$$

is the gain coefficient at the 5-n line centre frequency, ν_{5n}. As before N_{5n} represents the population inversion density on the 5-n transition.

If we assume that the gain medium (the strontium plasma) is reasonably uniform over the spatial range of interest, then the solution of equation (91) is straightforward and we can write

$$I_{5n}(z) = I_{5n}(o)e^{\alpha_{5n}z} + \frac{\varepsilon_{5n}\Delta\Omega}{\alpha}\left[e^{\alpha_{5n}z} - 1\right] \qquad (93)$$

where $I_{5n}(o)$ represents the irradiance (arising from emission on the 5-n transition) incident on the segment of plasma under consideration. Clearly enumeration of equation (93) is required in order to provide the appropriate stimulated rates, equation (87), that arise in the population rate equations. However, the equations are coupled as ε_{5n} and α_{5n} depend upon the appropriate population densities.

It is also apparent from equations (87) and (92) that we need to evaluate the effective bandwidth of the 5-n transition, Δ_{5n} $\{\equiv 1/L_{5n}\}$, which in turn depends upon the gain of medium. Yariv[37] indicates that in the case of an inhomogeneously broadened line the effective bandwidth for the unsaturated regime {i.e., $I_{5n} < I_{5n}^{S}$} is given by

$$\Delta_{5n} = \Delta\nu_{5n}^{D}\left[\frac{\ell n(\kappa_{5n}z) - \ell n\{\ell n\,\frac{1}{2}\,[\exp(\kappa_{5n}z) + 1]\}}{\ell n 2}\right]^{1/2} \qquad (94)$$

where $\Delta\nu_{5n}^{D}$ is the FWHM Doppler width for the 5-n transition and κ_{5n} is the incremental line centre gain constant in the limit of extreme inhomogeneous broadening and is defined by the relation

$$\kappa_{5n} = \frac{N_{5n}^{o}\, c^2 (\ell n 2)^{1/2} A_{5n}}{4\pi^{3/2} \nu_{5n}^2\, \Delta\nu_{5n}^{D}} \qquad (95)$$

Here N_{5n}^{o} $\{\equiv W_p N_o / A_5\}$ represents the unsaturated population inversion density for the 5-n transition. The saturated irradiance

$$I_{5n}^{S} \equiv \frac{h\nu_{5n}}{\sigma_{5n}\tau_{5n}} \qquad (96)$$

where σ_{5n} is the 5-n line centre stimulated emission cross-section and $\tau_{5n} \equiv 1/A_{5n}$. In the saturated regime {i.e., $I_{5n} > I_{5n}^{S}$} Yariv[37] shows that $\Delta_{5n} = \Delta\nu_{5n}^{D}$.

In a first attempt to model the growth of the radiation field on each of the 5-n transitions (n = 4, 3 and 2) resulting from three photon excitation of level 5, we have assumed that two photon ionization of strontium vapor produces a uniform column of ground state SrII ions. We further assumed that negligible laser power was absorbed in this process. The justification for this lies in the small amount of laser energy required for this purpose compared to that available. Although this calculation was somewhat simplified it shows that this assumption is reasonable for our preliminary model of the interaction.

We then divide this plasma column into a number of thin slabs and assume that within each slab conditions are uniform and equations (82) and (83) can be solved to describe the temporal variation of the level population densities subject to the radiation field present. It should be noted that we have implicitly assumed that the plasma density is sufficiently low that we can neglect collisional processes for the times of interest. Of particular concern is electron excitation of the 4^2D metastable term of SrII. In the case of a 30 ns laser pulse this requires the electron density to be no greater than 10^{15} cm^{-3}. If full ionization were achieved this implies that the strontium atom density prior to irradiation should be limited to about 10^{15} cm^{-3}.

The irradiance arising from the 5-n transition and emitted in the z-direction from the i^{th} slab of thickness Δz is given by

$$I_{5n}^{i} = I_{5n}^{i-1} e^{\alpha_{5n}^{i} \Delta z} + \frac{\varepsilon_{5n}^{i} \Delta\Omega}{\alpha_{5n}^{i}} \left[e^{\alpha_{5n}^{i} \Delta z} - 1 \right] \qquad (97)$$

where I_{5n}^{i-1} represents the incident irradiance, ε_{5n}^{i} the volume emission coefficient and α_{5n}^{i} the gain coefficient (corresponding to the 5-n transition) for the i^{th} slab. In the case of the first slab (i=1) we have

$$I_{5n}^{1} = \frac{\varepsilon_{5n}^{1} \Delta\Omega}{\alpha_{5n}^{1}} \left[e^{\alpha_{5n}^{1} \Delta z} - 1 \right] \qquad (98)$$

where $\Delta\Omega$ was set equal to the area of the ionized column divided by the square of the column length.

The laser irradiance used for our preliminary calculation approximated the experimental laser pulse and was given by the following expression:

$$I_L(t) = I_L^{max} e^{-\left(\frac{t-\tau_1}{\tau_2}\right)^2} \qquad (99)$$

where I_L^{max} represents the peak irradiance, τ_1 = 10 ns and $\tau_2 = \begin{cases} 6 \text{ ns for } t \leq 10 \text{ ns} \\ 12 \text{ ns for } t > 10 \text{ ns} \end{cases}$. Attenuation of the laser radiation arising from the near resonant three photon pumping of the strontium ion was also taken into account through the relation

$$\frac{dI_L(z,t)}{dz} = -\beta N_1 I_L^3(z,t) \qquad (100)$$

If we assume N_1 and β are uniform over the i^{th} slab thickness Δz, the solution of this equation yields

$$I_L^i = \frac{I_L^{i-1}}{\left[1 + 2\beta^i N_1^i (I_L^{i-1})^2 \Delta z\right]^{1/2}} \qquad (101)$$

The above set of equations has been solved by a 4th-order Runge-Kutta routine to yield the emission on each of the 5^2F-6^2D, 5^2F-5^2D and 5^2F-4^2D multiplets. The results of our preliminary calculations indicate that the equations are stiff and that a better computational routine DEGEER should be employed. Nevertheless, our initial calculations, performed for a column length of 0.2 mm, indicated appreciable emission on the 2.82 μm and 177 nm transitions as seen from figure 30. These results look encouraging for they suggest that laser action on the VUV line should be attainable. Currently we are improving our computer code in order to extend these comuptations to more practical lengths.

Experimental Program

In parallel with this theoretical work we have designed and assembled an experimental facility to both test this concept and study laser superelastic heating of an ionic resonance transition within a plasma. The former will be achieved by tuning the laser to 422.14 nm, while the latter will be accomplished by tuning the laser close to the 421.67 nm resonance line of SrII. In both cases the side light emission will be studied, but for the three photon experiment we also plan to monitor the emission coaxial with the pump laser beam.

The basic components of this facility are shown in figure 31 and include a crossed heat pipe, with four optical ports, that is designed to operate with strontium vapor. A vacuum blind phototube with a visible wavelength blocking filter will be used to monitor the vacuum ultraviolet emission at 177 nm while a photomultiplier coupled to a SPEX 1700II

monochromator will be used to monitor the yellow 562.4 nm emission. Our new Nd-YAG laser pumped dye laser will be used to pump the strontium vapor for both experiments. The signals from our photodetectors will be processed by our gated EGG signal averager.

At the time of writing this facility has just become operational and we have undertaken a preliminary experiment that involved scanning the dye laser from 0.3 nm to the red of 422.14 nm through to 0.3 nm to the blue of 421.67 nm. The axial emission at 562.4 nm was monitored during this experiment. Although a reasonable signal was observed it appeared that the vapor density was too high and the three photon generated emission at 562.4 nm was mixed into the tail of what appeared to be superelastically generated plasma emission associated with laser saturation of the 421.67 nm resonance line. These results are nevertheless encouraging for they suggest that both phenomena could indeed be studied. We are next planning a lower density run to optimize the conditions for the 3 photon scheme.

REFERENCES

1 T. B. Lucatorto and T. J. McIlrath, Phys. Rev. Letters, 37, 428-431, 1976.

2 T. J. McIlrath and T. B. Lucatorto, Phys. Rev. Letters, 38, 1390-1393, 1977.

3 C. H. Skinner, J. Phys. B: Atom. Molec. Phys., 13, 55-68, 1980.

4 D. J. Krebs and L. D. Shearer, J. Chem. Phys. 75, 3340-3344, 1981.

5 C. Bréchignac and Ph. Cahuzac, Optics Commun., 43, 270-273, 1982.

6 J. Krasinski, T. Stacewicz and C. R. Stroud Jr., Optics Commun. 33, 158-162, 1980.

7 D. J. Krebs and L. D. Shearer, J. Chem. Phys. 75, 3340-3344, 1981.

8 F. Roussel, P. Breger, G. Spiess, C. Manus and S. Geltman, J. Phys. B: Atom. Molec. Phys. 13, L631-L636, 1980.

9 T. Stacewicz and J. Krasinski, Optics Commun. 39, 35-40, 1981.

10 B. Carré, F. Roussel, P. Breger and G. Spiess, J. Phys. B: Atom. Molec. Phys. 14, 4289-4300, 1981.

11 B. Carré, F. Roussel, P. Breger and G. Spiess, J. Phys. B: Atom. Molec. Phys. 14, 4271-4288, 1981.

12 J. L. LeGouet, J. L. Picqué, F. Wuilleumier, J. M. Bizau, P. Dhez, P. Koch and D. L. Ederer, Phys. Rev. Lett., 48, 600-603, 1982.

13 J. Kumar, W. T. Silfvast and O. R. Wood II, J. Appl. Phys., 53, 218-222, 1982.

14 L. Jahreiss and M. C. E. Huber, Phys. Rev. A, 28, 3382-3401, 1983.

15 R. M. Measures, J. Quant. Spectrosc. Radiat. Transfer, 10, 107-125, 1970.

16 R. M. Measures, J. Appl. Phys., 48, 2673-2675, 1977.

17 R. M. Measures, N. Drewell and P. Cardinal, J. Appl. Phys., 50, 2662-2669, 1979.

18 R. M. Measures and P. G. Cardinal, Physical Review A, 23, 804-815, 1981.

19 R. M. Measures, P. G. Cardinal and G. W. Schinn, J. Appl. Phys. 52, 1269-1277, 1981, and 52, 7459, 1981.

20 R. M. Measures, "Laser Resonance Saturation: An Efficient and Rapid Means of Ionization and Electron Heating". Invited paper at the

Society for Optical and Quantum Electronics LASER'S 82 Meeting, New Orleans, Dec. 12-17, 1982.

21 R. M. Measures, N. Drewell and P. Cardinal, Appl. Optics, 18, 1824-1827, 1979.

22 R. G. Caro, J. C. Wang, R. W. Falcone, J. F. Young and S. E. Harris, Appl. Phys. Lett., 42 9-11, 1983.

23 J. Bokor, R. R. Freeman and W. E. Cooke, Phys. Rev. Lett., 48, 1242-1245, 1982.

24 E. J. Morgan and R. D. Morrison, Phys. Fluids, 8, 1608, 1965.

25 An. N. Nesmeyanov, "Vapour Pressure of the Elements (Translator, J. I. Carasso), Academic Press, 1963.

26 S. K. Wong and R. M. Measures, UTIAS Report No. 292, 1985.

27. H. R. Griem, "Spectral Line Broadening by Plasmas", Academic Press, New York, 1974.

28 M. Mitchner and C. Kruger, "Partially Ionized Gases", Wiley Interscience, 1974.

29 A. Vinagradov, I. Sobelman and E. Yukov Sov. J. Quantum Electron, 5, 59-63, 1975.

30 T. P. Apruzese, J. Davis and K. G. Whitney, J. Phys. B: Atom. Molec. Phys. 11, L643-L649, 1978.

31 I. Matheni, E. M. Campbell and P. Hagelstein, Energy, Tech. Rev. 23-31, 1983.

32 J. Trebow and M. Krishnan, Phys. Rev. Lett., 28, 679-682, 1983, and IEEE Journal of Quantum Electron. QE-19, 1870-1873, 1983.

33 R. C. Elton, Opt. Eng. 21, 307-312, 1982.

34 R. H. Dixon and R. C. Elton, J. Opt. Soc. Am. B/1, 232-238, 1984.

35 R. M. Measures, P. L. Wizinowich and P. G. Cardinal, J. Appl. Phys. 51, 3622-3628, 1980.

36 A. Yariv, IEEE J. Quant. Electron. QE-13, 943, 1977.

37 A. Yariv, "Quantum Electronics", 2nd Ed., Wiley, 1975.

CUMULATIVE CHRONOLOGICAL LIST OF PUBLICATIONS (1979-PRESENT)

1. R. M. Measures, M. A. Cappelli, P. G. Cardinal and S. K. Wong, "Laser Off Resonance Maximum Absorption (LORMA) Effect Observed in Sodium Vapor" (in preparation 1985).
2. S. K. Wong and R. M. Measures, "Three Dimensional Mapping of Laser Ionization Based on Resonance Saturation" (in preparation).
3. M. A. Cappelli, P. G. Cardinal, H. Hechen and R. M. Measures, "Sodium Atom Distribution Within a Heat Sandwich Oven" (accepted for publication in Rev. Sci. Inst., 1985).
4. M. A. Cappelli and R. M. Measures, "Two Channel Technique for Stark Measurements of Electron Density Within a Laser Produced Sodium Plasma", Appl. Optics 23, 2107-2114, 1984.
5. G. W. Schinn and R. M. Measures, "STROPE - A New Species Density Gradient Measurement Technique", Appl. Optics 23, 1258-1266, 1984.
6. R. M. Measures, "Laser Resonance Saturation: An Efficient and Rapid Means of Ionization and Electron Heating", Invited Paper in the Proc. of Soc. for Optical and Quantum Electronics LASERS 82 Meeting, New Orleans, Dec. 12-17, 1982.
7. R. M. Measures and H. Herchen, "Laser Absorption Under Saturation Conditions with Allowance for Spectral Hole Burning", J. Quant. Spectrosc. Radiat. Transfer 29, 9-18, 1983.
8. R. M. Measures, S. K. Wong and P. G. Cardinal, "The Influence of Molecular Nitrogen Upon Plasma Channel Formation by Laser Resonance Saturation", J. Appol. Physics 53, 5541-5551, 1982.
9. M. R. Arnfield and R. M. Measures, "Ion to Neutral Atom Measurements within an Ablation Plasma Through Laser Selective Excittion Spectroscopy", Physical Review A, 24 535-539, 1981.
10. R. M. Measures, P. G. Cardinal and G. W. Schinn, "Theoretical Model of Laser Ionization of Alkali Vapours Based on Resonance Saturation", J. Appl. Phys. 52, 1269-1277, 1981.
11. P. G. Cardinal, P. L. Wizinowich and R. M. Measures, "Anomalous Laser Ener;gy Absorption Associated with Resonance Saturation", J. Quant. Spectrosc. Radiat. transfer 25, 537-545, 1981.

12. R. M. Measures and P. G. Cardinal, "Laser Ionization Based on Resonance Saturation - A Simple Model Description", Physical Review A, 23, 804-815, 1981.
13. R. M. Measures, P. L. Wizinowich and P. G. Cardinal, "Fast and Efficient Plasma Heating Through Superelastic Laser Energy Conversion", J. Appl. Phys., 51, 3622-3628, 1980.
14. H. S. Kwong and R. M. Measures, "Lifetime Measurements on Atoms in Compounds Embedded in Matrices Using Laser Selective Excitation and Ablation Dynamics", Appl. Optics, 19, 1025-1027, 1980.
15. R. M. Measures, N. Drewell and P. Cardinal, "Electron- and Ion-Beam Transportation Channel Formation by Laser Ionization Based on Resonance Saturation - LIBORS", J. Appl. Phys. 50, 2622-2669, 1979.
16. R. M. Measures, N. Drewell and P. Cardinal, "Laser Interaction Based on Resonance Saturation (LIBORS): An Alternative to Inverse Bremsstrahlung for Coupling Laser Energy into a Plasma", Appl. Optics, 18, 1824-1827, 1979.
17. H. S. Kwong and R. M. Measures, "Trace Element Laser Microprobe Having High Sensitvity and Freedom from Chemical Matrix Effects", Analytical Chemistry, 51, 428-432, 1979.
18. R. M. Measures and H. S. Kwong, "Development of a Trace Element Analyser Based on Laser Ablation and Selective Excitated Radiation - TABLASER", Appl. Optics, 18, 281-285, 1979.

Books

1. R. M. Measures, "Laser Remote Sensing", J. Wiley & Sons, 1984.
2. R. M. Measures, "Analytical Use of Lasers in Remote Sensing", Chapter 6 of Analytical Laser Spectroscopy (Ed. N. Omenetto), J. Wiley Publications, 1979.

PROFESSIONAL PERSONNEL

Principal Investigator:

Dr. R. M. Measures (Professor of Applied Science and Engineering)

Research Assistants:

P. G. Cardinal (Ph.D. Student)

R. S. Kissack (Ph.D. Student)

S. K. Wong (Ph.D. Student)

M. A. Cappelli (Ph.D. Student)

K. Menard (M.A.Sc. Student)

K. Spariosu (M.A.Sc. Student)

S. D. Hanratty (M.A.Sc. Student)

P. Gomes (M.A.Sc. Student)

Interactions

Professor R. M. Measures has been asked to serve on the Program Committee of the newly formed "International Laser Science Conference", first meeting to be held November 18-22, 1985, Dallas, Texas.

NEW DISCOVERIES STEMMING FROM RESEARCH

Saturation of an atomic transition by the intense radiation field of a suitably tuned laser represents an important kind of interaction with a wide range of potential applications. The consequences of laser resonance saturation and the applications stemming from this interaction depend to a very large extent upon the period of saturation. If the resonance to ground level populations are only momentarily locked in the ratio of respective degeneracies (saturation) the principal effect is a burst of intensified spontaneous emission that can be used to diagnose the excited medium.[1,2] On the other hand an extended period of saturation (lasting for much longer than the resonance state lifetime) can lead to extensive perturbation of the medium.[3,4] Indeed, if the free electron superelastic collision time is short compared to the duration of the laser pulse near total ionization of the laser pumped species is rapidly achieved.[4-19] In the case of an ionic species extremely rapid changes of electron temperature can be produced by this means.[20]

The author was the first to recognize the importance of laser saturation and many of its possible areas of application.[1-4] Subsequent work in the author's laboratory and elsewhere have proven that laser resonance saturation does represent a significant form of interaction between laser radiation and atomic vapours or plasmas.

Momentary laser saturation represents a powerful diagnostic technique that is finding application in many areas ranging from fusion reactor studies[21] to combustion measurements.[22,23] The combination of laser ablation and laser saturation spectroscopy represents a new approach at evaluating fundamental atomic quantities such as: radiative lifetimes, branching ratios, transition probabilities and selected collision cross-sections. A preliminary paper on this subject was published by us in Physical Review.[24] This technique, as well as being convenient and accurate, is particularly well suited for measurements on short lived, highly ionized species created by laser ablation. Furthermore, it is versatile and can use multiphoton or stepwise excitation as the means of generating the bursts of intensified emission.

As a spin-off of this work we have also shown that this concept can also form the basis of a new form of trace element laser microprobe called a TABLASER.[25]

More recently, we have demonstrated in a proof of principle experiment that laser saturation spectroscopy can be used to directly measure, with both spatial and temporal resolution, the ion to neutral atom density ratio in a rapidly expanding ablation plasma.[26]

The ionization capabilities of extended laser resonance saturation have now been indisputably demonstrated with a variety of experiments.[5-17] We have developed a model of this laser ionization based on resonance saturation (LIBORS) and have shown that the interaction can be thought to proceed in four stages.[18,19] Confirmation of certain aspects of our theory has been provided by several research groups.[5-17] Recently, there has been some success in using laser resonance saturation for the purpose of creating infrared laser action.[27] Currently, our efforts are concentrating upon obtaining a better understanding of this interaction and in studying how best to employ this fast and very efficient method of coupling laser energy into a plasma for the purpose of developing an efficient short wavelength laser.

1. R. M. Measures, J. Appl. Phys. 39, 5232-5245 (1968).
2. R. M. Measures, Phys. of Fluids, 13, 1889-1890 (1970).
3. R. M. Measures, J. Quant. Spectrosc. Radiat. Transfer, 10, 107-125 (1970).
4. R. M. Measures, J. Appl. Phys., 48, 2673-2675 (1977)
5. T. B. Lucatorto and T. J. McIlrath, Phys. Rev. Letters, 37, 428-431 (1976).
6. T. J. McIlrath and T. B. Lucatorto, Phys. Rev. Letters, 38, 1390-1393 (1977).
7. C. H. Skinner, J. Phys. B: Atom. Molec. Phys., 13, 55-68 (1980).
8. F. Roussel, P. Breger, G. Spiess, C. Manus and S. Geltman, J. Phys. B: Atom. Molec. Phys., 13, L631-L636 (1980).
9. T. Stacewicz, Optics Commun. 35, 239-241 (1980).
10. C. H. Skinner, J. Phys. B: Atom. Molec. Phys., 13, L637-L640 (1980).
11. J. Krasinski, T. Stacewicz and C. R. Stroud Jr., Optics Commun. 33, 158-162 (1980).
12. D. J. Krebs and L. D. Shearer, J. Chem. Phys., 75, 3340-3344 (1981).
13. T. Stacewicz and J. Krasinski, Optics Commun., 39, 35-40 (1981).

14. B. Carré, F. Roussel, P. Breger and G. Spiess, J. Phys. B: Atom. Molec. Phys., 14, 4289-4300 (1981).
15. B. Carré, F. Roussel, P. Breger and G. Spiess, J. Phys. B: Atom. Molec. Phys., 14, 4271-4288 (1981).
16. J. L. LeGouet, J. L. Picque, F. Muilleumier, J. M. Bizau, P. Shez, P. Koch and D. L. Ederer, Phys. Rev. Lett., 48, 600-603 (1982).
17. J. Kumar, W. T. Silfvast and O. R. Wood II, J. Appl. Phys., 53, 218-222 (1982).
18. R. M. Measures and P. G. Cardinal, Physical Review A, 23, 804-815 (1981).
19. R. M. Measures, P. G. Cardinal, G. W. Schinn, J. Appl. Phys., 52, 1269-1277 (1981) and 52, 7459 (1981).
20. R. M. Measures, P. L. Wizinowich and P. G. Cardinal, J. Appl. Phys., 51, 3622-3628 (1980).
21. C. H. Muller and K. H. Burrell, Phys. Rev. Lett., 47, 330-333 (1981).
22. J. D. Bradshaw, N. Omenetto, G. Zizak, J. N. Bower and J. D. Winefordner, Appl. Optics, 19, 2709-2716 (1980).
23. G. B. Boutilier, N. Omenetto and J. D. Winefordner, Appl. Optics, 19, 1838-1843 (1980).
24. R. M. Measures, N. Drewell and H. S. Kwong, Phys. Rev. A, 16, 1093-1097 (1977).
25. R. M. Measures and H. S. Kwong, Appl. Optics, 18, 281-286 (1979).
26. M. R. Arnfield and R. M. Measures, Phys. Rev. A, 24, 535-539 (1981).
27. W. Muller and I. V. Hertel, Appl. Phys., 24, 33-38 (1981).

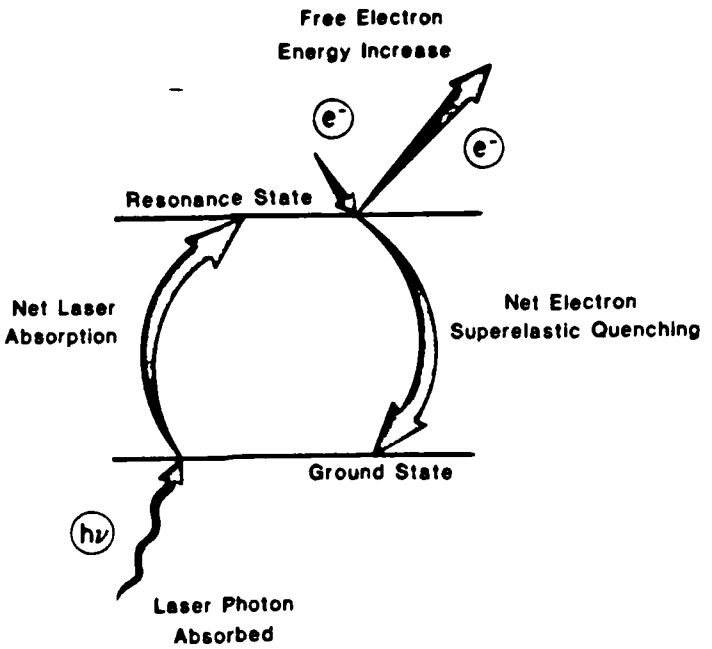

FIG. 1 SUPERELASTIC ELECTRON HEATING THROUGH LASER RESONANCE SATURATION OF SODIUM ATOMS.

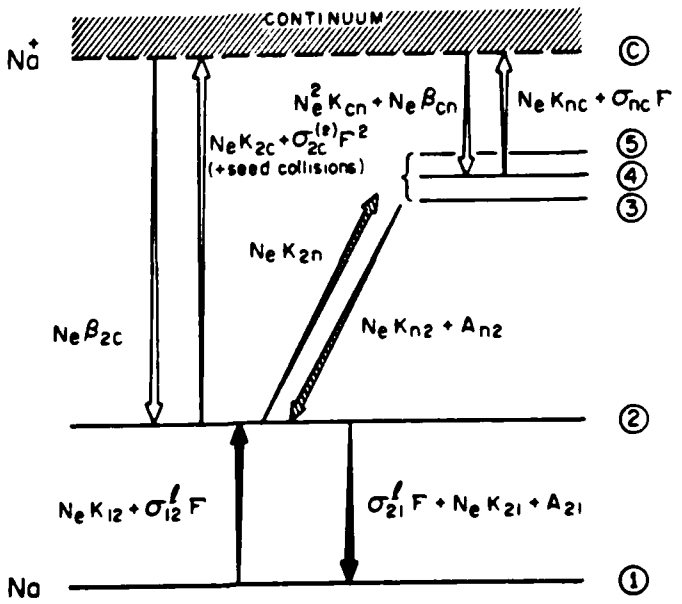

FIG. 2 BASIC COLLISIONAL-RADIATIVE MODEL USED IN 5 LEVEL-LIBORS CODE.

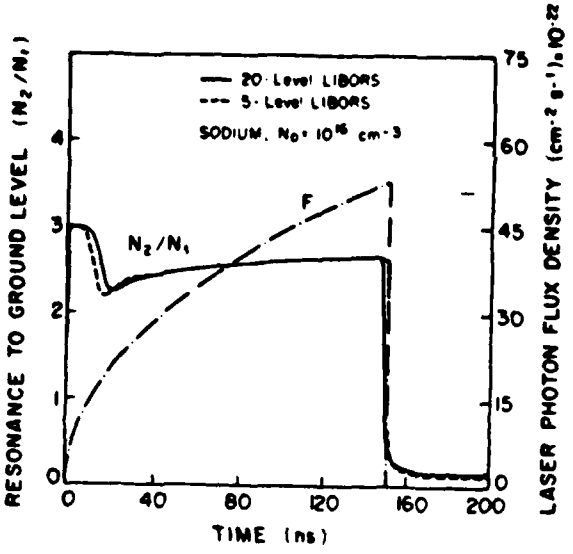

(a)

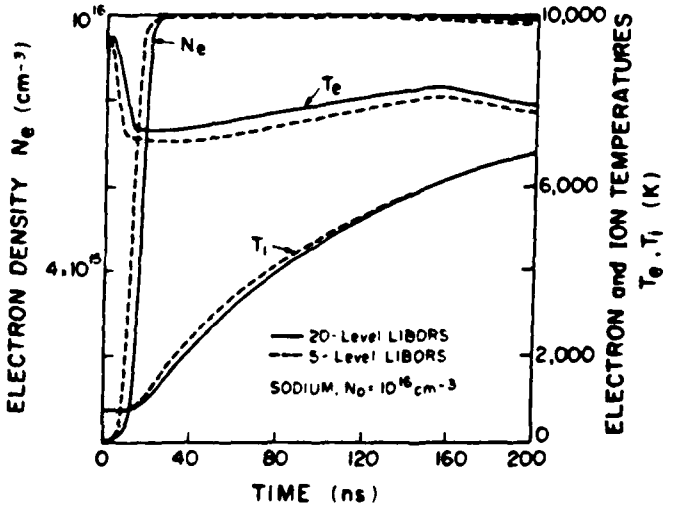

(b)

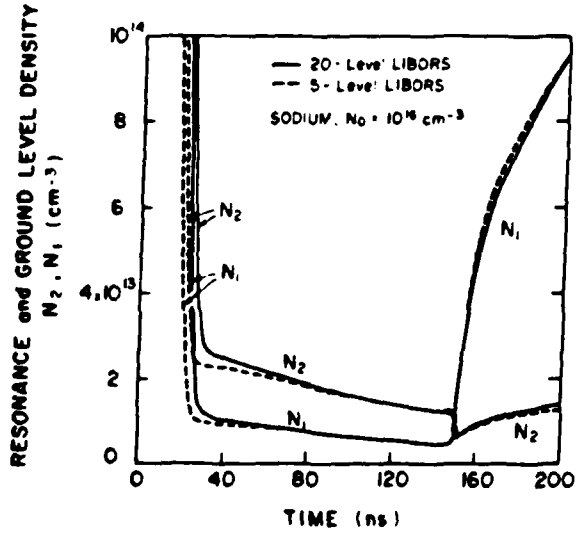

(c)

FIG. 3 COMPARISON OF 20- AND 5-LEVEL LIBORS COMPUTER CODES FOR SODIUM ATOM DENSITY OF 10^{16} CM^{-3}.

(a) Temporal Variation of N_2/N_1 for the Truncated Laser Pulse Indicated by F (Photons cm^{-2} sec^{-1}).

(b) Temporal Variation of N_e, T_e and T_i for the same F.

(c) Temporal Variation of N_2, N_1 for the same F.

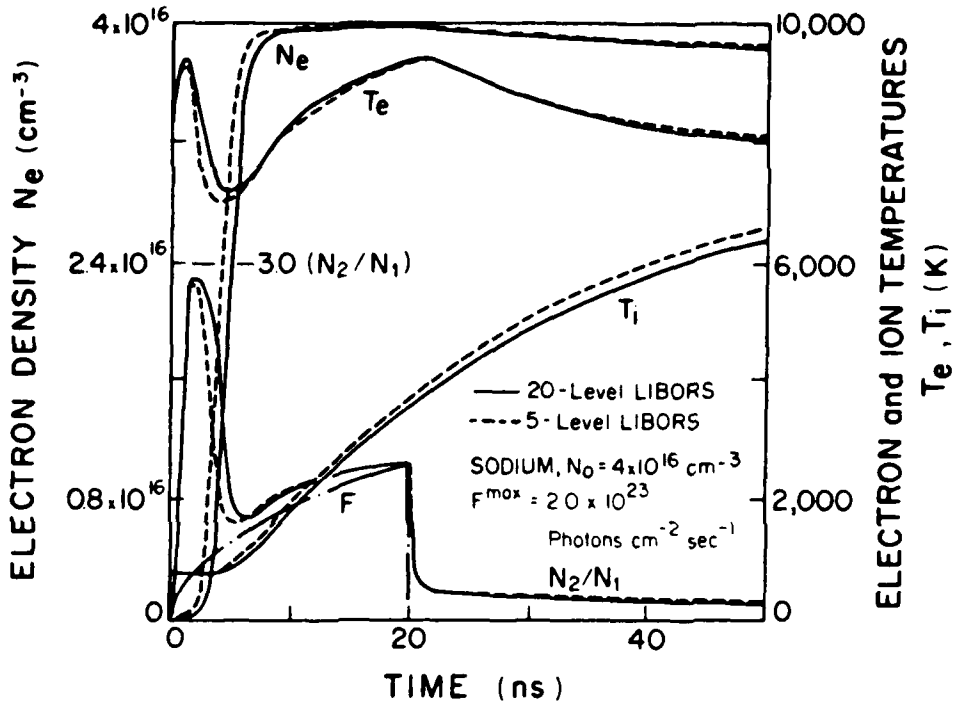

FIG. 4 COMPARISON OF 20 AND 5-LEVEL LIBORS COMPUTER CODE PREDICTIONS OF TEMPORAL VARIATIONS IN Ne, Te, Ti and N_2/N_1 FOR LASER PHOTON FLUX DENSITY F. NOTE SATURATION LIMIT FOR N_2/N_1 IS 3.

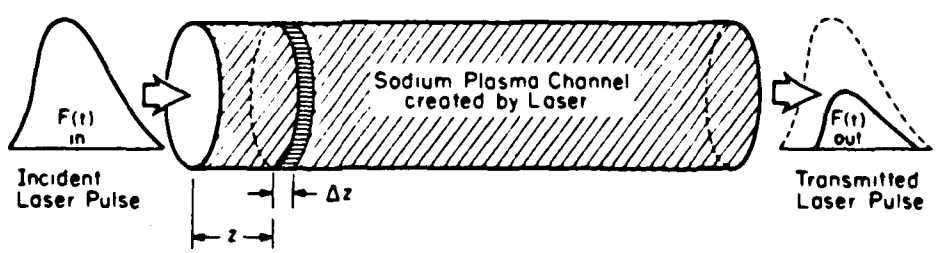

FIG. 5 ATTENUATION AND TEMPORAL DISTORTION OF LASER PULSE AS IT PROPAGATES THROUGH SODIUM VAPOR CAUSING IONIZATION THROUGH RESONANCE SATURATION. F(t) IS THE LASER PHOTON FLUX DENSITY.

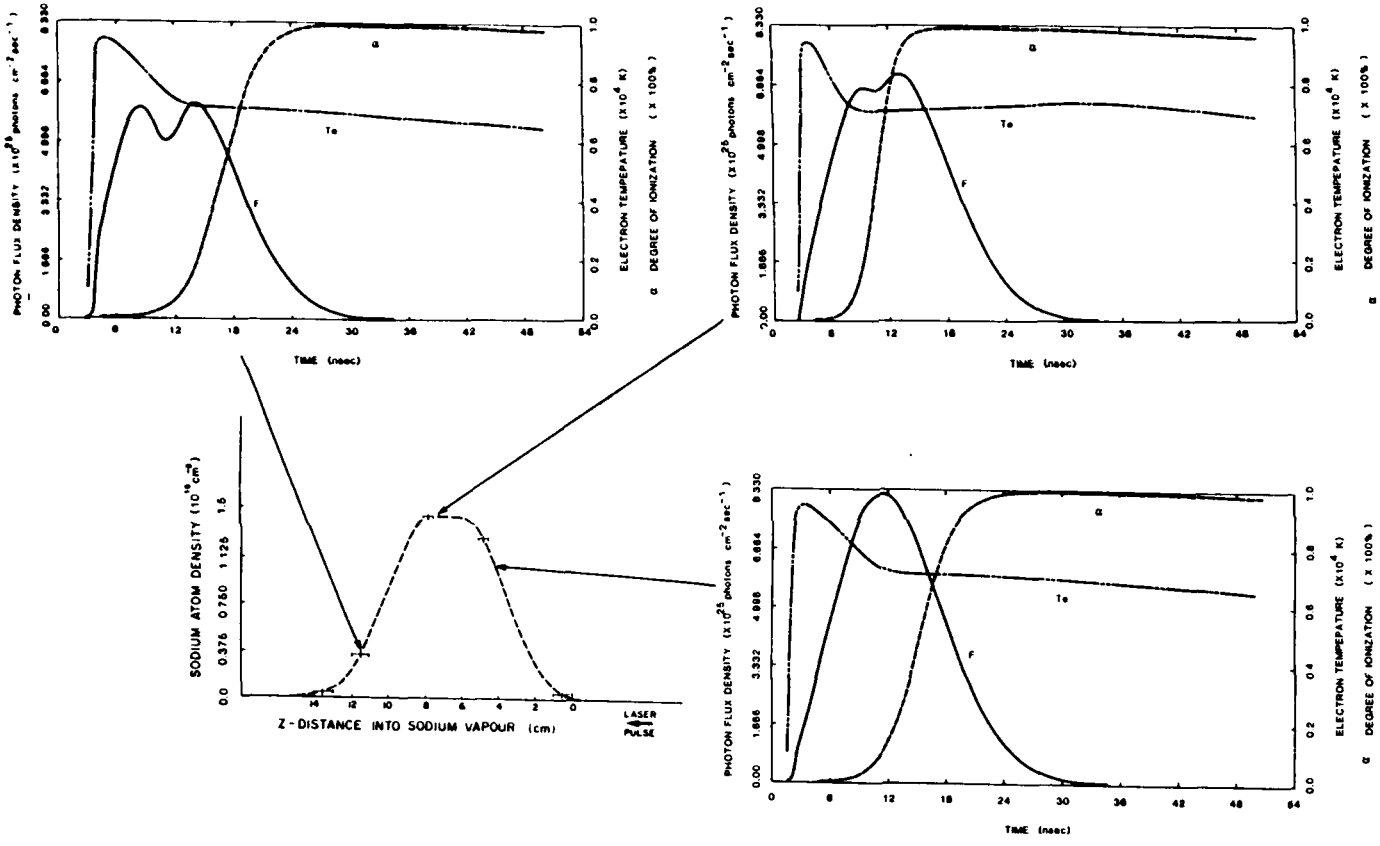

FIG. 6 COMPUTED TEMPORAL BEHAVIOUR OF THE ELECTRON TEMPERATURE T_e, DEGREE OF IONIZATION α AND THE LASER PHOTON FLUX DENSITY AT THREE LOCATIONS ALONG THE SODIUM VAPOR COLUMN. LOWER LEFT FIGURE DISPLAYS MEASURED SODIUM ATOM RADIAL DISTRIBUTION WITHIN HEAT SANDWICH OVEN.

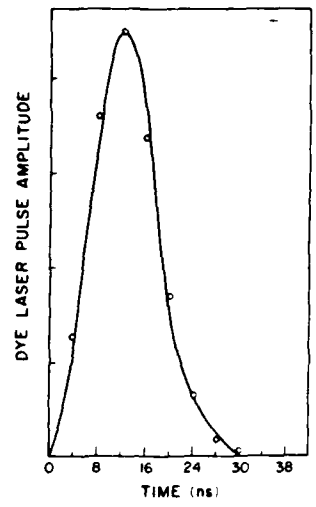

FIG. 7 COMPARISON OF EXPERIMENTAL LASER PULSE AND EMPIRICAL FIT USED IN LIBORS CODE.

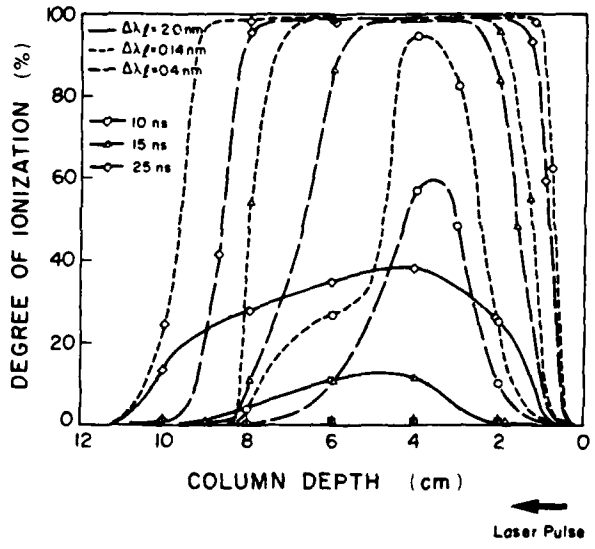

FIG. 8 5E-LIBORS CODE PREDICTION OF THE VARIATION IN THE DEGREE OF IONIZATION OF SODIUM VAPOR ALONG PATH OF LASERS FOR THREE INSTANTS OF TIME CORRESPONDING TO THREE VALUES OF LASER DETUNING.

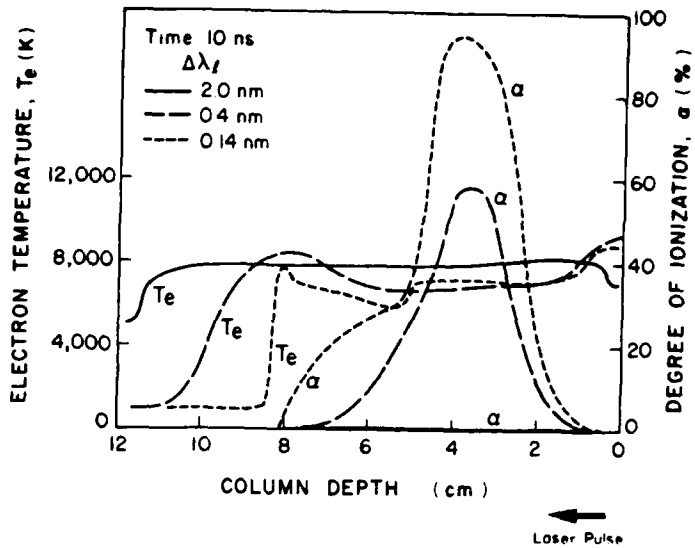

FIG. 9 COMPUTED VARIATION OF ELECTRON TEMPERATURE T_e AND DEGREE OF IONIZATION α ALONG PATH OF LASER PULSE 10 NS AFTER START OF INCIDENT IRRADIATION FOR THREE SETTINGS OF LASER DETUNING.

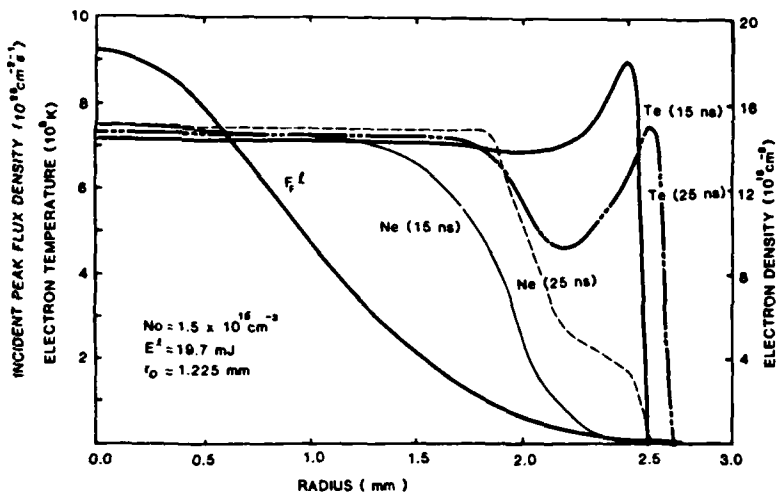

FIG. 10 COMPUTED RADIAL VARIATION OF ELECTRON TEMPERATURE T_e AND ELECTRON DENSITY N_e FOR 10 AND 25 NS AFTER START OF INCIDENT IRRADIATION FOR A 19.7 mJ LASER PULSE (DETUNED BY 0.14 NM) WITH A GAUSSIAN RADIAL DISTRIBUTION.

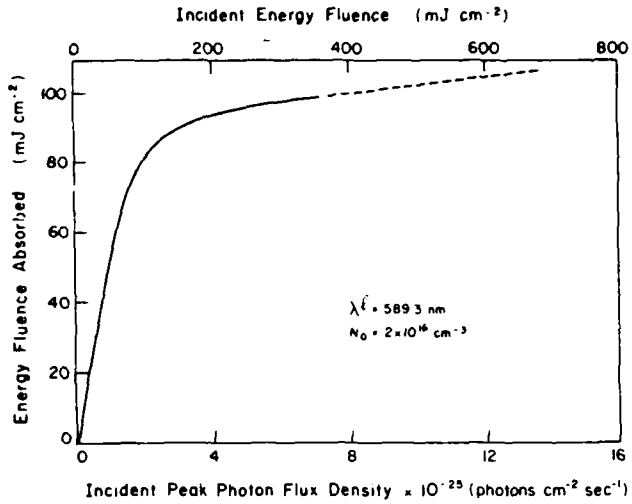

FIG. 11 COMPUTED VARIATION OF ABSORBED LASER ENERGY FLUENCE WITH INCIDENT PEAK PHOTON FLUX DENSITY (AND ENERGY FLUENCE) FOR λ_ℓ = 589.3 NM AND PEAK SODIUM DENSITY OF 2×10^{16} CM^{-3}.

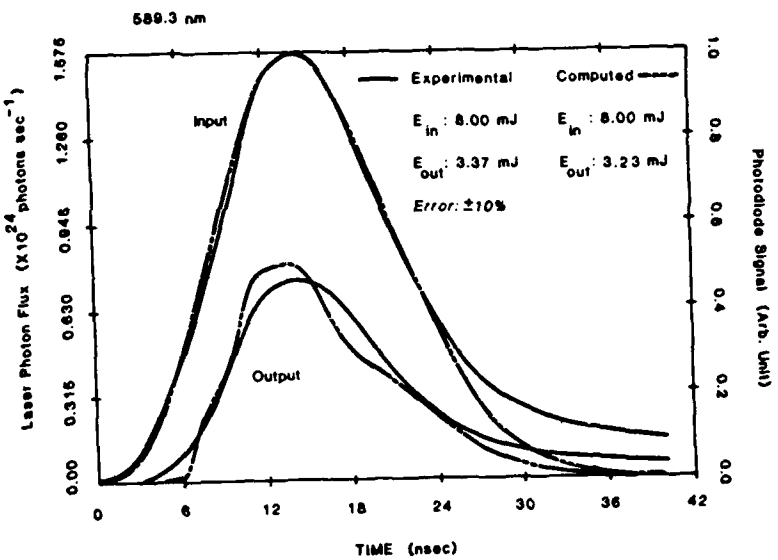

FIG. 12 COMPARISON OF EXPERIMENTAL AND COMPUTED INCIDENT AND TRANSMITTED LASER PHOTON FLUX DENSITY FOR λ_ℓ = 589.3 NM AND PEAK SODIUM DENSITY OF 1.5×10^{16} CM^{-3}.

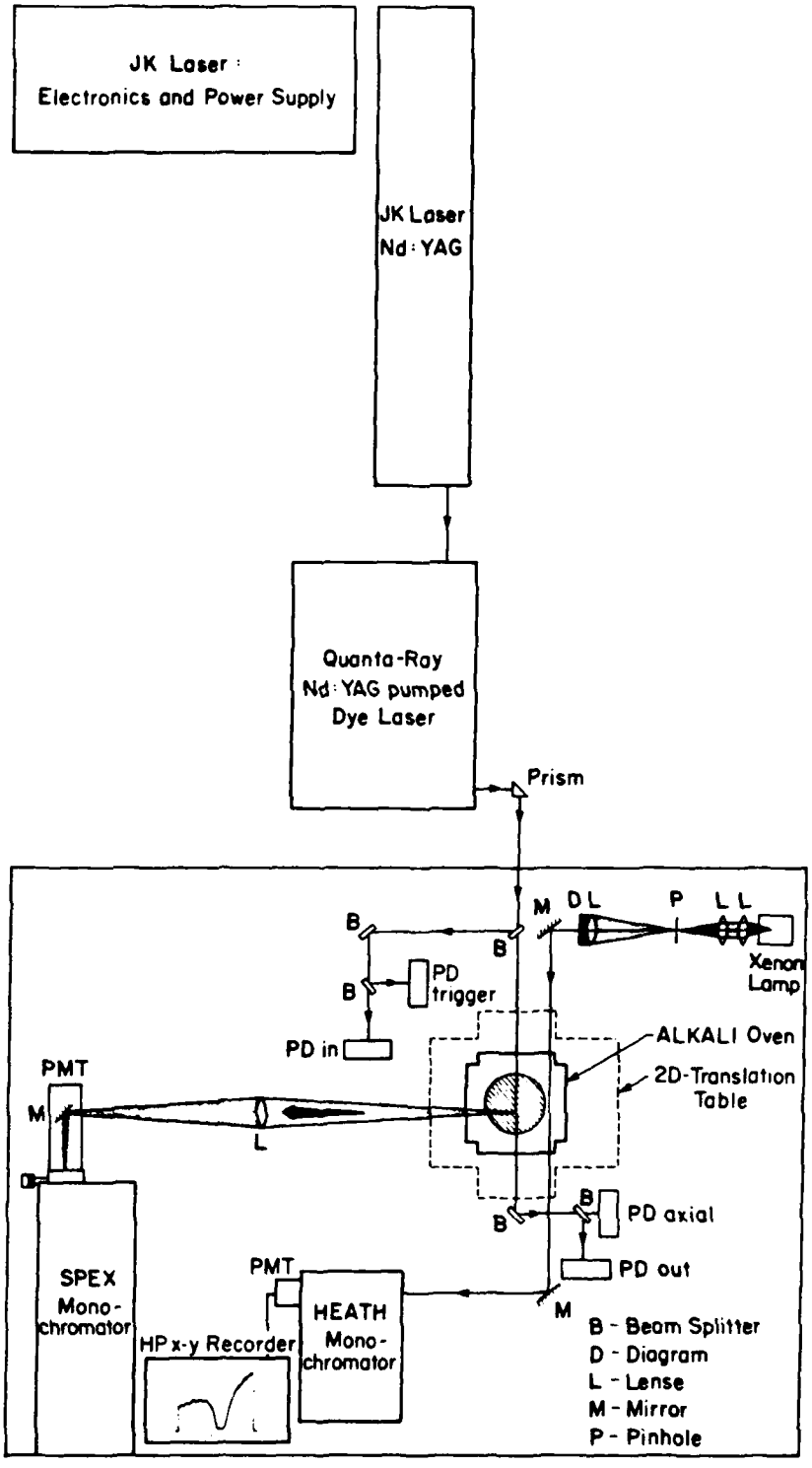

FIG. 13 SCHEMATIC OVERVIEW OF NEW Nd-YAG LASER DRIVEN LIBORS FACILITY.

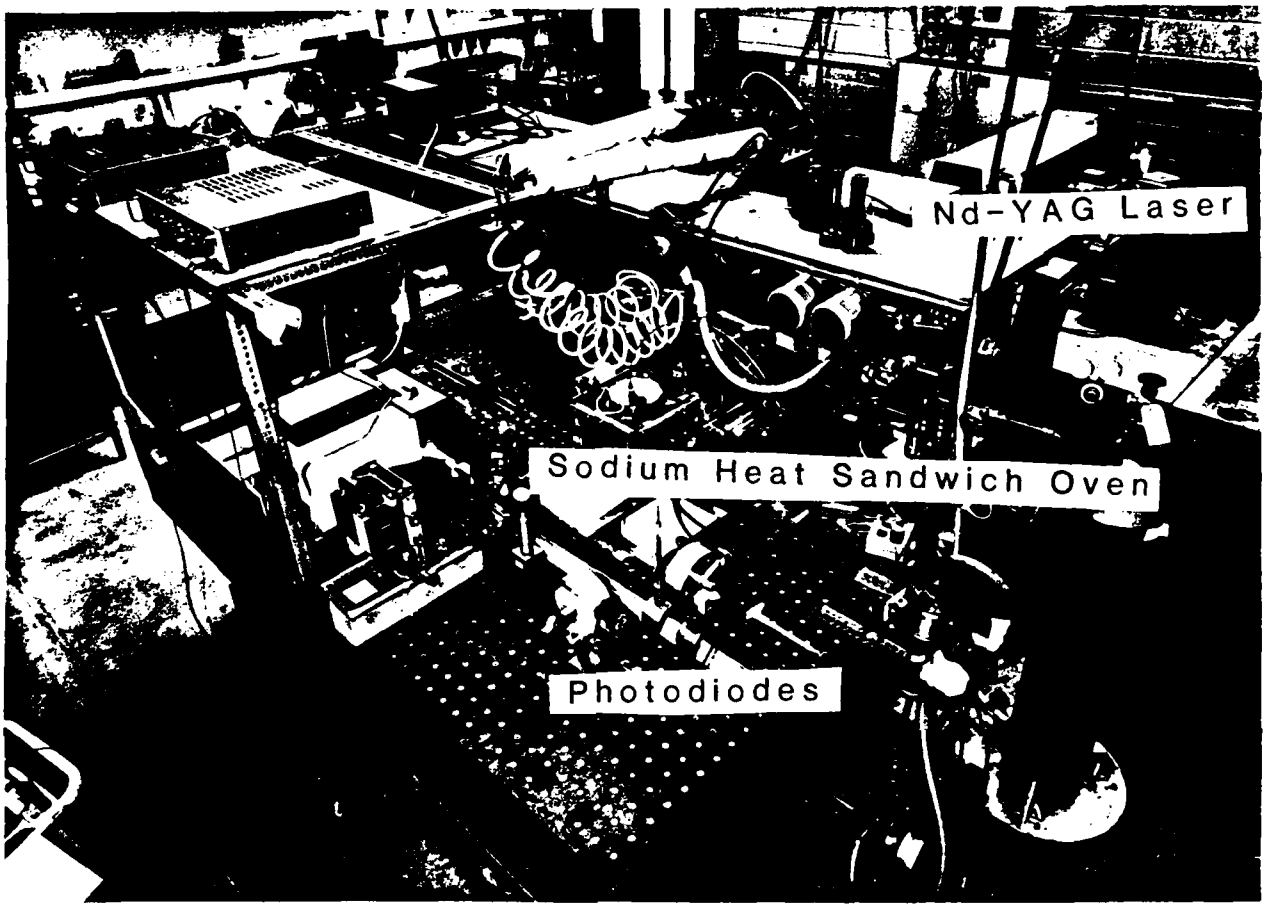

FIG. 14 PICTURE OF LIBORS FACILITY SHOWING HEAT SANDWICH OVEN AND PHOTODETECTION SYSTEM ON GRANITE TABLE IN FOREGROUND AND Nd-YAG LASER IN BACKGROUND.

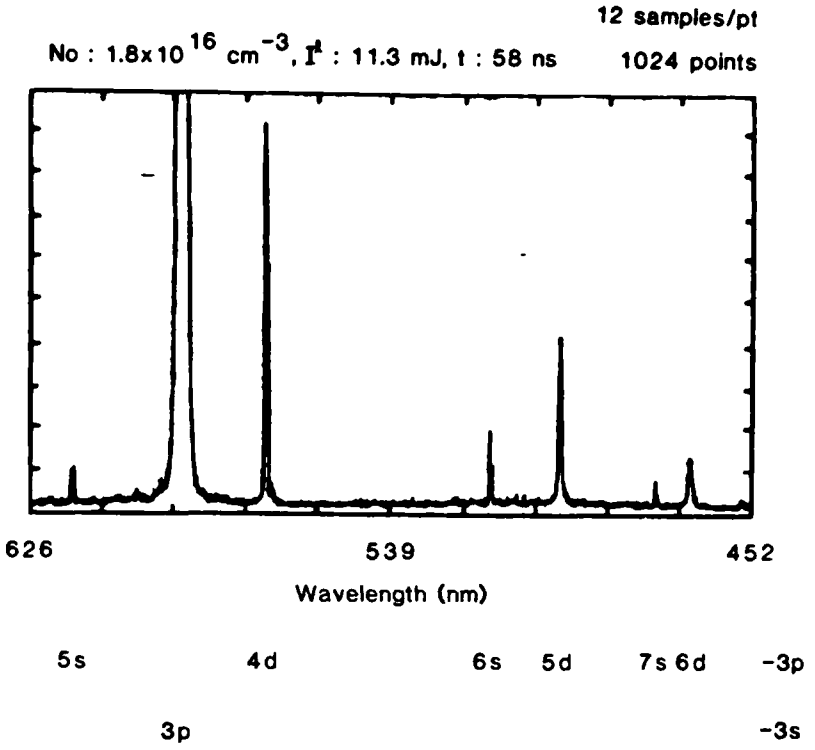

FIG. 15 SPECTRAL SCAN OF EMISSION FROM SODIUM PLASMA CREATED BY LASER RESONANCE SATURATION.

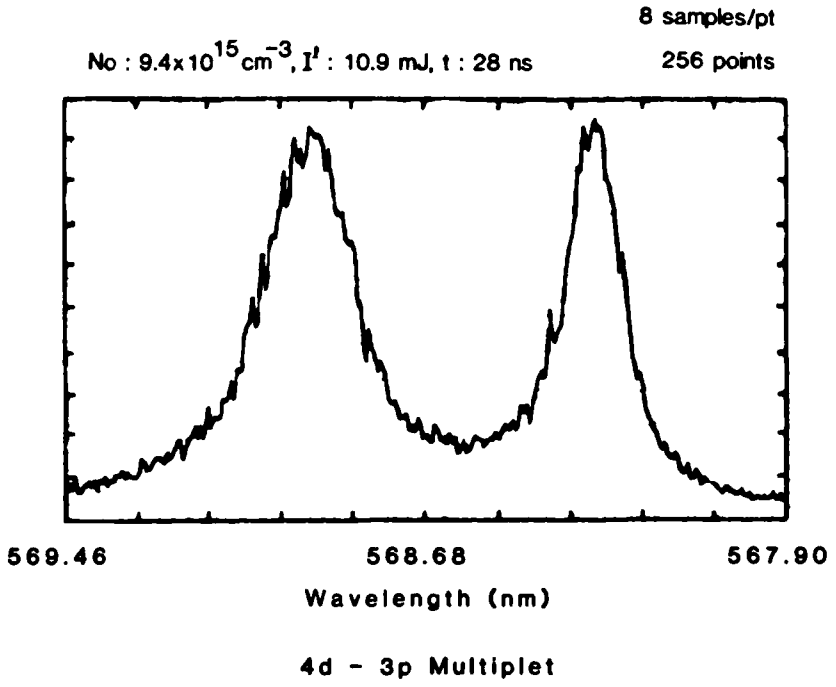

FIG. 16 HIGH RESOLUTION SPECTRAL SCAN OF THE 4^2D-3^2P MULTIPLET FROM SODIUM PLASMA CREATED BY LASER RESONANCE SATURATION.

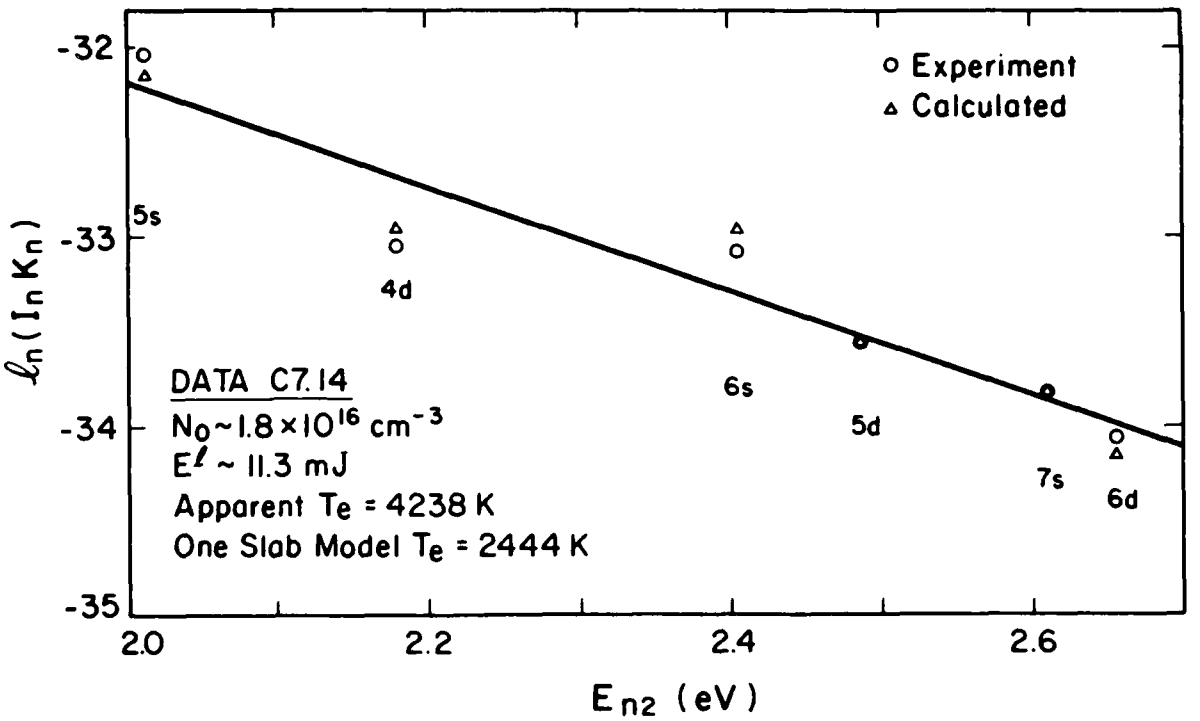

FIG. 17 LOG PLOT OF EXPERIMENTAL LINE EMISSION FROM SODIUM PLASMA (O). ALSO SHOWN IS BEST LINEAR FIT TO DATA AND COMPUTED LINE EMISSION FOR A ONE SLAB OPTICALLY THICK MODEL (Δ).

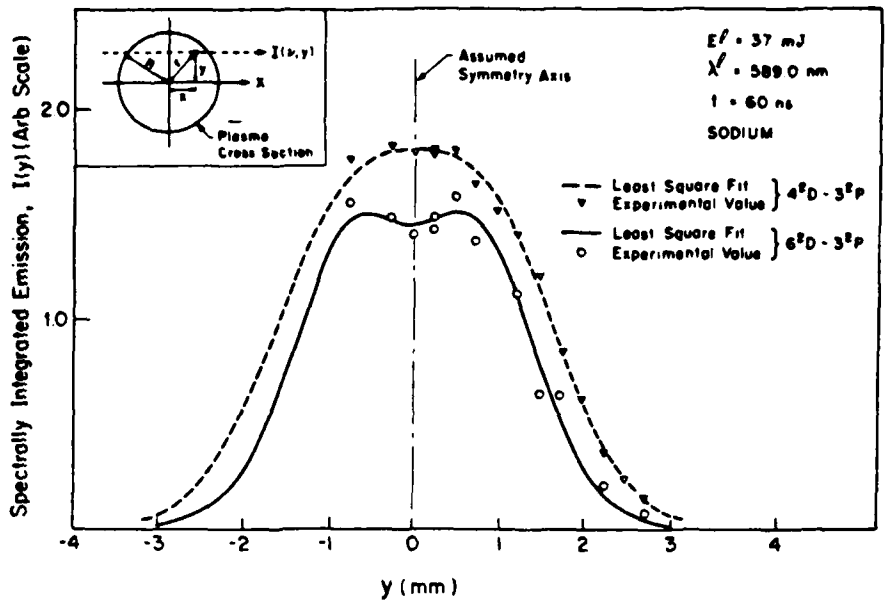

FIG. 18 EXPERIMENTALLY MEASURED RADIAL DISTRIBUTION OF SODIUM EMISSION ON $4\,^2D-3\,^2P$ (— —) AND $6\,^2D-3\,^2P$ (——) MULTIPLETS.

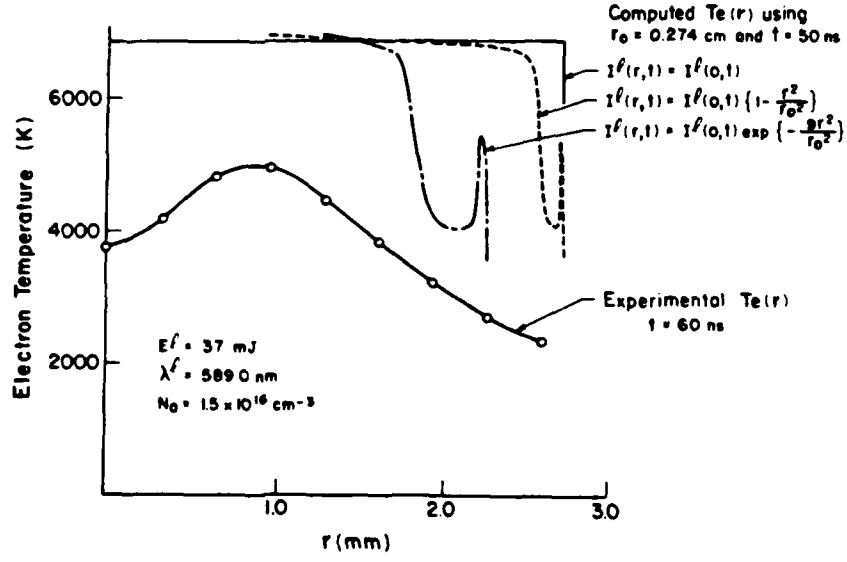

FIG. 19 DECONVOLUTED RADIAL ELECTRON TEMPERTURE DISTRIBUTION MEASURED AT 60 NS FROM ONSET OF LASER IRRADIANCE FROM CENTRE OF SODIUM HEAT SANDWICH OVEN. ALSO SHOWN ARE THREE THEORETICAL RADIAL TEMPERATURE DISTRIBUTIONS BASED ON LIBORS CODE FOR THREE DIFFERENT LASER RADIAL PROFILES.

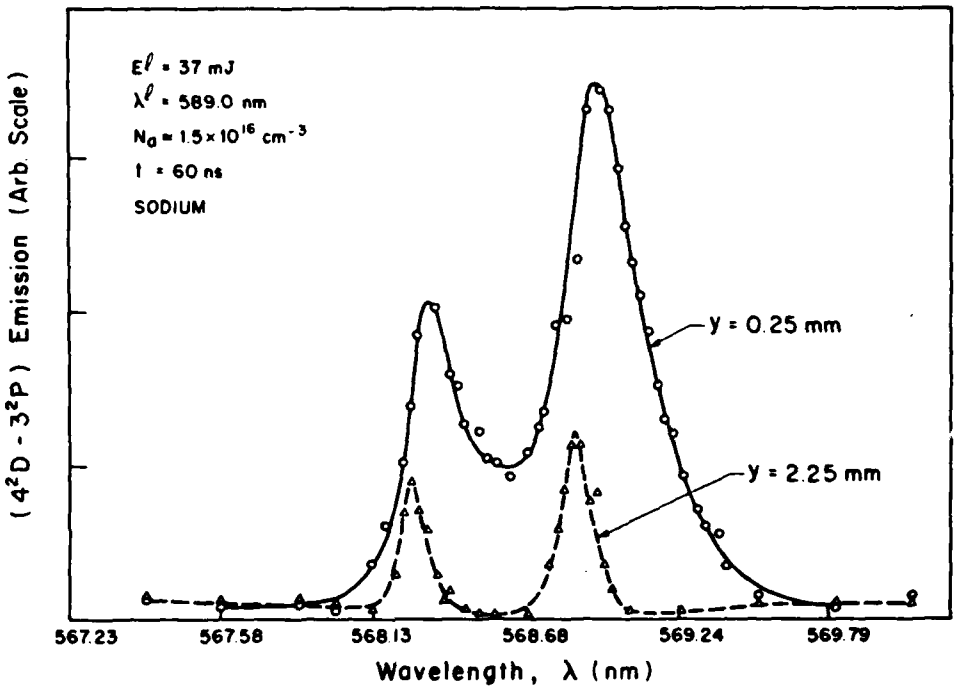

FIG. 20 TWO SPECTRAL PROFILES OF SODIUM $4\,^2D$-$3\,^2P$ MULTIPLET, EXPERIMENTALLY MEASURED CLOSE TO THE LASER BEAM AXIS (y = 0.125 MM) AND IN WING OF PLASMA (y = 2.25 MM).

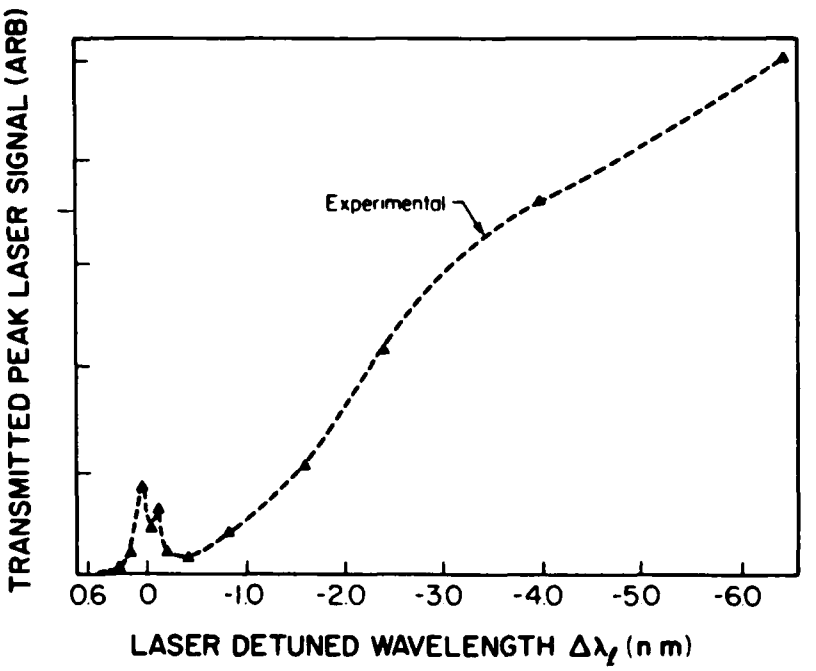

FIG. 21 VARIATION OF EXPERIMENTALLY MEASURED PEAK TRANSMITTED LASER PULSE AS FUNCTION OF DETUNING MAXIMUM SODIUM DENSITY IN SANDWICHED OVEN WAS 4×10^{16} CM^{-3}.

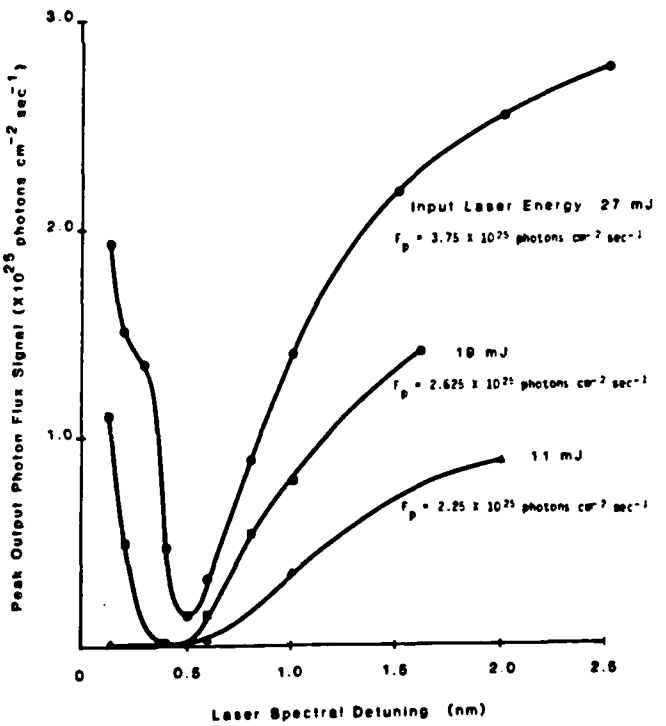

FIG. 22 COMPUTED VARIATION OF TRANSMITTED PEAK LASER PHOTON FLUX DENSITY AGAINST LASER SPECTRAL DETUNING FOR THREE VALUES OF INCIDENT LASER ENERGY. PEAK SODIUM DENSITY 4×10^{16} CM^{-3}.

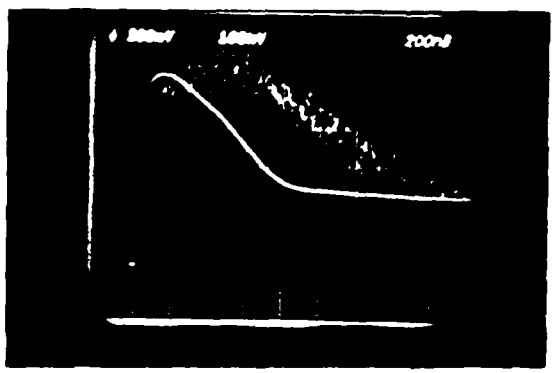

(b)

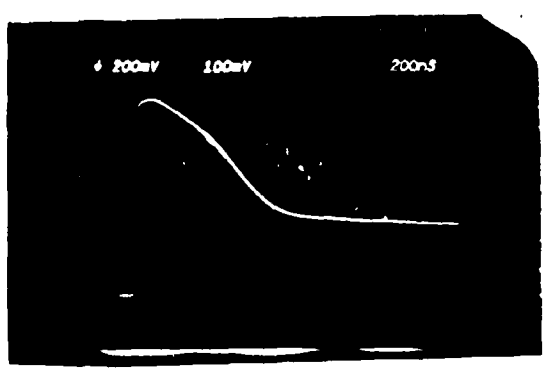

(a)

FIG. 23 COMPARISON OF SODIUM PLASMA RECOMBINATION RADIATION IN 5 NM BAND CENTRED ABOUT 405 NM WHEN (A) LASER TUNED TO 589.6 NM SODIUM RESONANCE LINE AND (B) LASER DETUNED TO 590.1 NM.

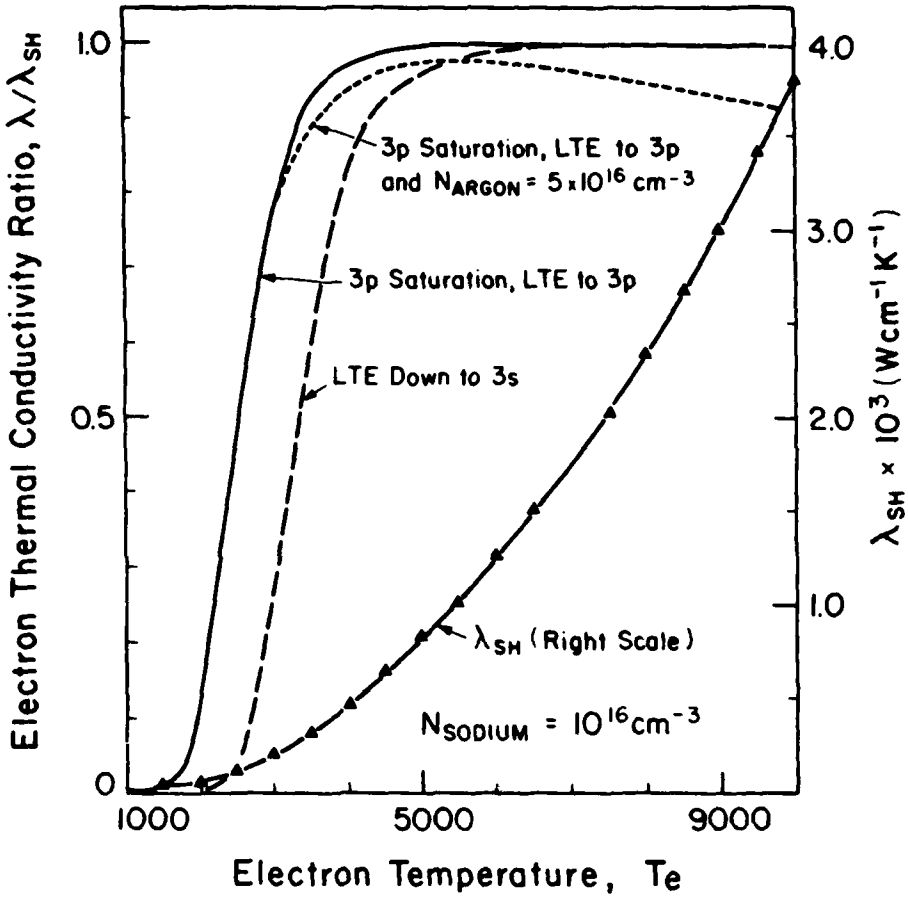

FIG. 24 COMPUTED RATIO OF ELECTRON THERMAL TRANSPORT COEFFICIENT λ OVER SPITZER-HARM VALUE λ_{SH} AS FUNCTION OF ELECTRON TEMPERATURE T_e FOR THREE THEORETICAL MODELS. ALSO SHOWN IS VARIATION OF λ_{SH} WITH T_e.

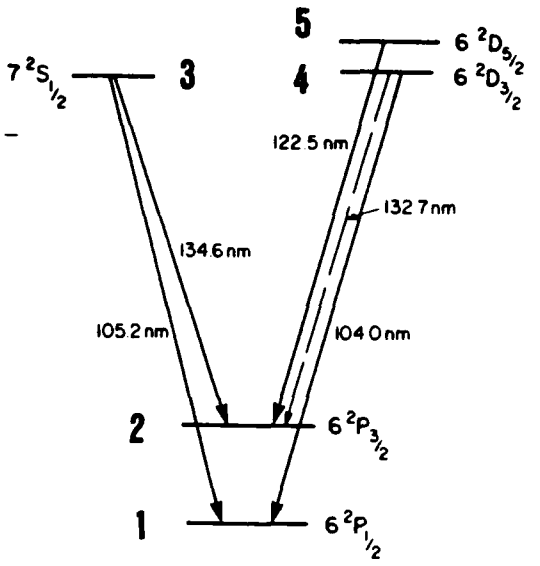

FIG. 25 BiIII PARTIAL GROTIAN DIAGRAM.

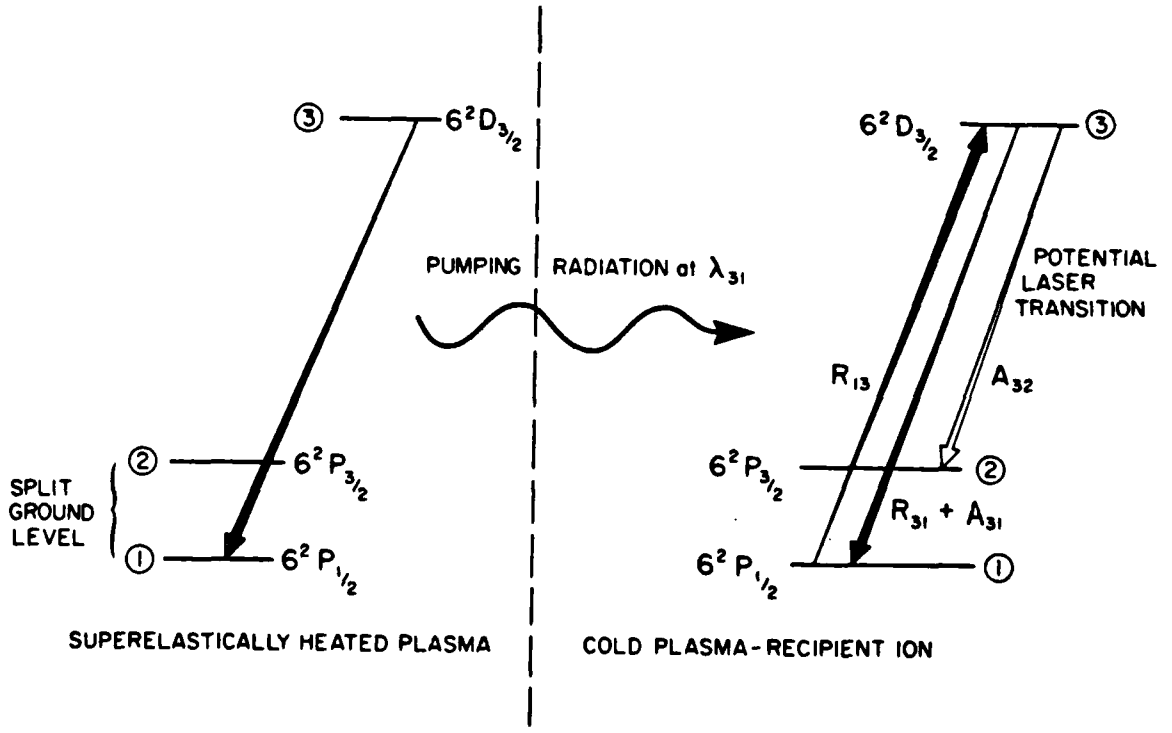

FIG. 26 NEW SELF-PUMPING RESONANCE INVERSION SPRI-CONCEPT FOR SHORT WAVELENGTH LASER.

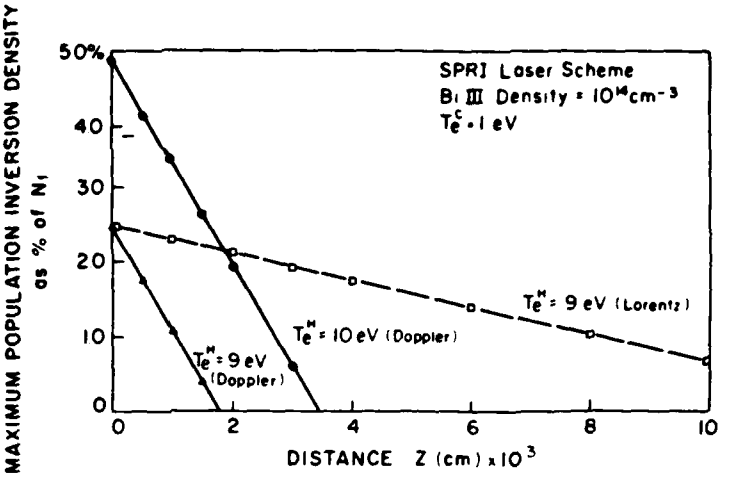

FIG. 27 MAXIMUM NORMALIZED INVERTED POPULATION DENSITY AS FUNCTION OF PENETRATION DEPTH INTO 1 eV COLD BiIII PLASMA FOR BOTH DOPPLER AND LORENTZ ABSORPTION PROFILES.

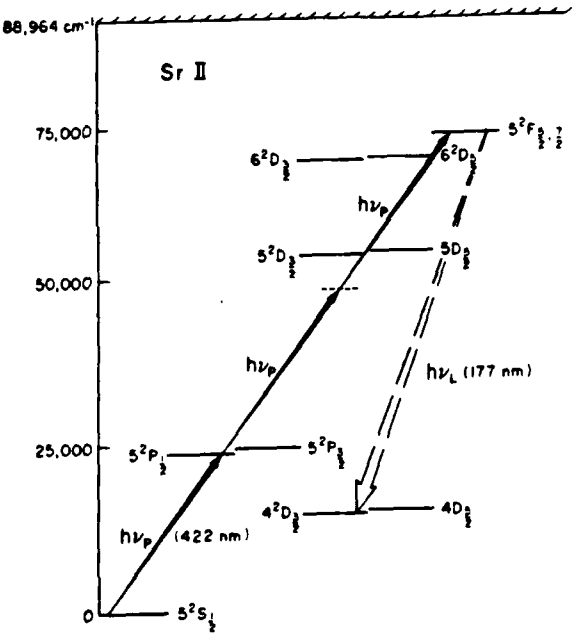

FIG. 28 SCHEMATIC REPRESENTATION OF NEW THREE PHOTON SATURATION LASER SCHEME ILLUSTRATED FOR STRONTIUM ION WITH 422 NM PUMPING. POTENTIAL VUV LASER TRANSITION AT 177 NM.

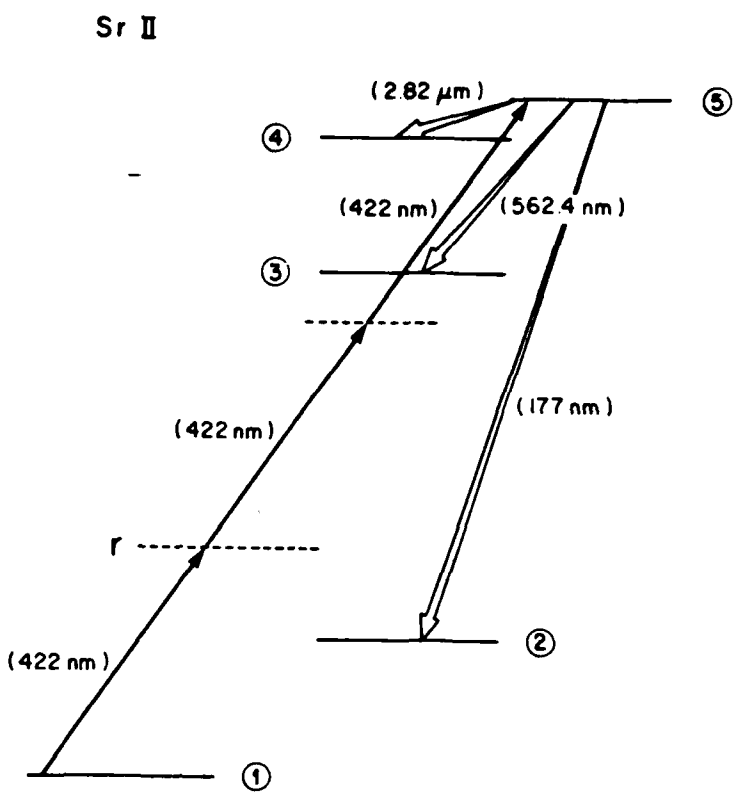

FIG. 29 SCHEMATIC MODEL USED IN COMPUTING LASER POTENTIAL OF THREE PHOTON SATURATION CONCEPT IN STRONTIUM SHOWING THREE COMPETING LASER TRANSITIONS AT 2.82 μM, 562.4 NM AND 177 NM.

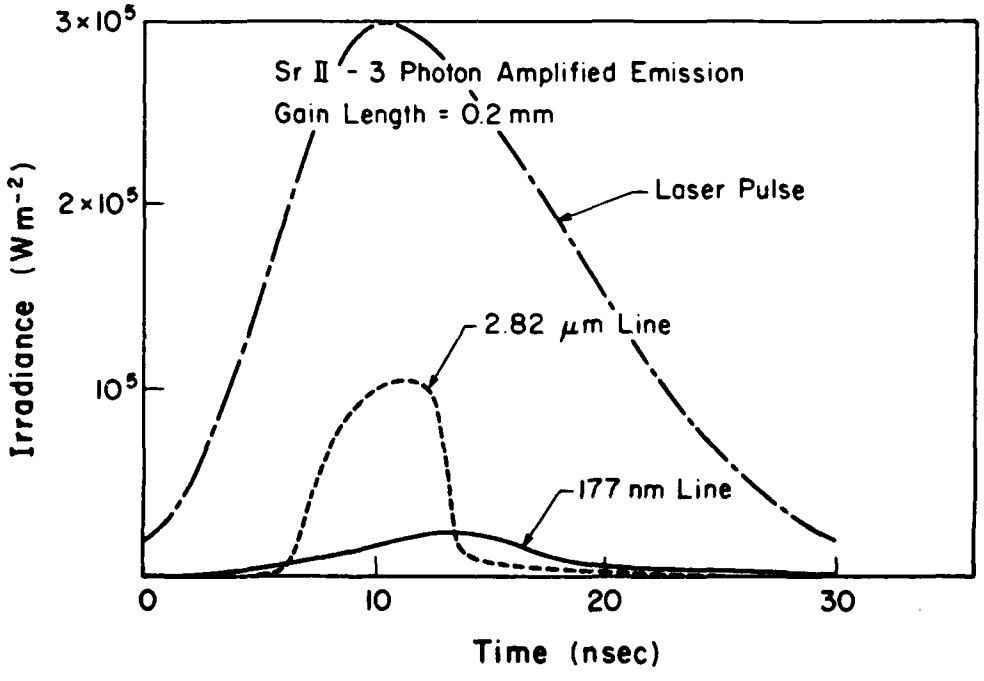

FIG. 30 COMPUTED EMISSION ON THE 2.82 μM AND 177 NM TRANSITIONS OF SrII RESULTING FROM IRRADIATION WITH SELF-NORMALIZED LASER PULSE SHOWN. LASER PEAK IRRADIANCE WAS 1×10^{8}W CM^{-2}.

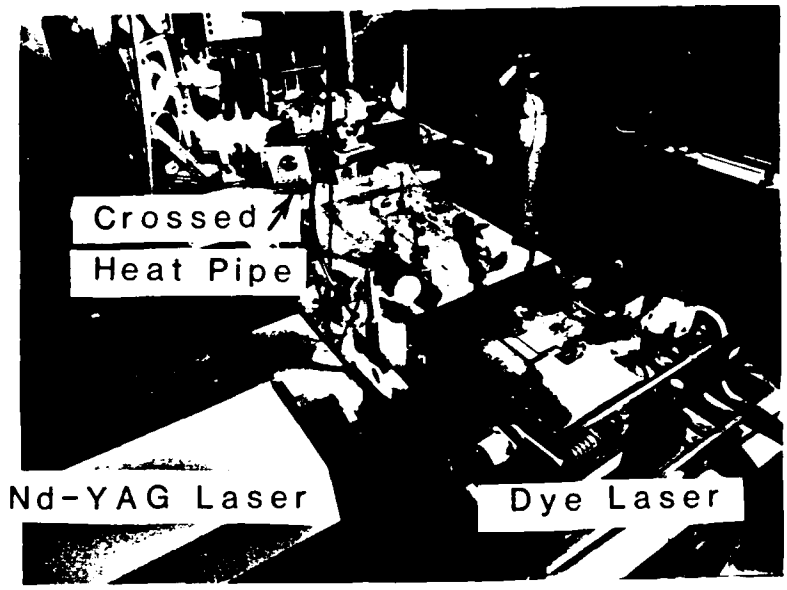

FIG. 31 NEW THREE PHOTON SATURATION FACILITY SHOWING STRONTIUM HEAT CROSS IN BACKGROUND AND Nd-YAG LASER PUMPED DYE LASER IN FOREGROUND.

Appendix A

Physical Mechanism for LORMA-Effect

In an attempt to explain in a simple manner the "laser off resonance maximum absorption" (or LORMA)-effect we shall assume that a near dynamic balance between laser absorption and superelastic electron quenching collisions determines the resonance and ground level populations of the sodium atoms. We further assume that the free electron density N_e is high enough that $N_e K_{21} >> A_{21}$ and we can neglect spontaneous decay of the resonance level populations. Consequently, we can write

$$(gN_1 - N_2)R_{21} \simeq N_e(N_2K_{21} - N_1K_{12}) \qquad (A1)$$

An order of magnitude calculation on the terms of the one dimensional radiative transfer equation (27) reveals that to good approximation

$$\frac{dI^{\ell}}{dz} \simeq (N_2 - gN_1)R_{21}E_{21} \qquad (A2)$$

where I^{ℓ} is the laser irradiance and E_{21} the resonance state energy. Combining the above equations leads us to state that the energy extracted per unit volume from the laser pulse

$$\Delta E^{\ell} \simeq \int_0^{\tau^{\ell}} N_e(N_2K_{21} - N_1K_{12})E_{21}dt \qquad (A3)$$

where τ^{ℓ} is the duration of the laser pulse.

In general equation (A1) can be written in the form

$$\frac{N_2}{N_1} = \frac{g(S_I + e^{-E_2/kT_e})}{S_I + 1} \qquad (A4)$$

where $S_I \equiv R_{21}/N_e K_{21}$ and is termed the "saturation parameter". If the

transition is saturated,

$$S_I >> 1 \text{ and } N_2 \approx gN_1 \tag{A5}$$

Furthermore our LIBORS codes clearly indicate that $e^{-E_{21}/kT_e} << 1$ and that the variation in K_{21} is small enough over the times of interest that we can write

$$\Delta E^{\ell} \approx K_{21}E_{21} \int_0^{\tau^{\ell}} N_2(t)N_e(t)dt \tag{A6}$$

Under saturation conditions, the bulk of the atomic populations reside in either the ground or resonance levels and so we can also assume

$$N_2(t) \approx G[N_o - N_e(t)] \tag{A7}$$

where $G = g/(1+g)$ and N_o is the original (prior to laser irradiance) atom density. If we further assume that the growth of the ionization is exponential then we can write

$$N_e(t) = \alpha N_o(1 - e^{-t/\tau}) \tag{A8}$$

where α is the "limiting degree of ionization" and τ is defined as the "ionization time".

Under these circumstances

$$\Delta E^{\ell} \approx GN_o{}^2K_{21}E_{21}f(\alpha, \tau^{\ell}/\tau) \tag{A9}$$

where

$$f(\alpha, \tau^{\ell}/\tau) = \alpha^2\tau \int_0^{t^{\ell}/\tau} [(\tfrac{1-\alpha}{\alpha}) + e^{-x}](1 - e^{-x})dx \tag{A10}$$

Integration yields

$$f(\alpha, \tau^{\ell}/\tau) = \alpha^2\tau[\frac{1}{2} + (\frac{\tau^{\ell}}{\tau} - 1) - (\frac{2\alpha-1}{\alpha})e^{-\tau^{\ell}/\tau} + \frac{1}{2} e^{-2\tau^{\ell}\tau}] \qquad (A11)$$

When the laser is only slightly detuned from resonance $\tau << \tau^{\ell}$ and $\alpha \approx 1$. In which case

$$f(\alpha, \tau^{\ell}/\tau) \approx \frac{1}{2} \tau\alpha^2 \qquad (A12)$$

and clearly the laser absorption increases with increased detuning because τ increases with increased detuning while α does not change appreciably.

For large detuning of the laser, $\tau >> \tau^{\ell}$ and $\alpha << 1$. Under these conditions

$$f(\alpha, \tau^{\ell}/\tau) \approx (1 - \alpha)\alpha\tau^{\ell} \qquad (A13)$$

and it is apparent that laser absorption now decreases with increased detuning because α becomes smaller with increased detuning. Also for large detuning the assumption of resonance saturation is expected to break down. It is thus clear that there will exist some small value of detuning for which the laser attenuation is a maximum if electron superelastic collision quenching plays a key role in the extraction of energy from the laser pulse.

END

FILMED

6-85

DTIC